Stratospheric Aerosol Intervention Experiment for the Chemistry-Climate Model Intercomparison Project

Simone Tilmes[1], Ewa M. Bednarz[2,3], Andrin Jörimann[4,5], Daniele Visioni[6], Douglas E. Kinnison[1], Gabriel Chiodo[7], and David Plummer[8]

[1]Atmospheric Chemistry, Observations, and Modeling Laboratory, National Center for Atmospheric Research, Boulder, CO, USA
[2]Cooperative Institute for Research in Environmental Sciences (CIRES), University of Colorado Boulder, Boulder, CO, USA
[3]NOAA Chemical Sciences Laboratory, Boulder, CO, USA
[4]Physikalisch-Meteorologisches Observatorium Davos / World Radiation Center, Davos, Switzerland
[5]Institute for Particle Physics and Astrophysics, ETH Zürich, Zürich, Switzerland
[6]Sibley School for Mechanical and Aerospace Engineering, Cornell University, Ithaca, NY, USA
[7]Instituto de Geociencias, Spanish National Research Council (IGEO-CSIC-UCM), Madrid
[8]Climate Research Branch, Environment and Climate Change Canada, Montréal, Canada

Correspondence: Simone Tilmes (tilmes@ucar.edu)

Abstract.

A new Stratospheric Aerosol Intervention (SAI) experiment has been designed for the Chemistry- Climate Modeling Initiative (CCMI-2022) to assess the impacts of SAI on stratospheric chemistry and dynamical responses and inter-model differences using a constrained setup with a prescribed stratospheric aerosol distribution and fixed sea-surface temperatures (SSTs) and

5 sea-ice. This paper describes the details of the experimental setup and the prescribed aerosol distribution. Furthermore, we discuss differences in the Whole Atmosphere Community Climate Model (WACCM6) results between the interactive stratospheric aerosol configuration with coupling to land, ocean, and sea ice that was used to produce the stratospheric aerosol distribution and the results of the constrained SAI experiment. With this, we identify and isolate the stratosphere-controlled SAI-induced impacts from those influenced by the coupling with the ocean. We confirm earlier suggestions that the SAI-induced positive

10 phase of the Northern Atlantic Oscillation in winter, with the corresponding winter warming over Eurasia, is directly driven by the effect of SAI on the stratosphere-troposphere coupling. We further show that the resulting stratospheric responses are largely similar between the fully coupled and constrained experiments, demonstrating the suitability of the simplified setup to study impacts in the stratosphere in a multi-model framework. Only small differences arise in the stratospheric ozone and dynamical SAI responses between the two experiments due to minor differences in the aerosol distributions and their coupling

15 with local changes in temperatures, upwelling, and chemistry, alongside interactive coupling with the ocean and sea ice.

1 Introduction

Recent studies have identified significant impacts of sulfur-based Stratospheric Aerosol Injections (SAI) on the stratosphere and below due to its effects on atmospheric chemistry, dynamics, and radiation (e.g., WMO, 2022). However, model-internal

differences resulted in a significant inter-model spread in the simulated SAI responses, including differences in aerosol loading,
20   distribution, and the resulting climate feedbacks (Pitari et al., 2014; Tilmes et al., 2022). Furthermore, only very few Earth
System Models (ESMs) that are interactively coupled with the ocean and cryosphere can interactively simulate stratospheric
aerosols, chemistry, and dynamics in the atmosphere, as is required for the recent Geoengineering Model Intercomparison
Project (GeoMIP) experiments (Visioni et al., 2023).

A multi-model intercomparison study by Tilmes et al. (2022), which investigated the impacts of SAI on the stratospheric
25   composition and ozone, was based on the GeoMIP G6sulfur and G6solar experiments. This experiment used the CMIP6 SSP5-
85 high-end greenhouse gas (GHG) forcing scenario (Meinshausen et al., 2017) as a baseline. It required sulfur injections into
the tropical lower stratosphere ($10°N – 10°S$) to produce global mean surface temperatures close to those simulated for the
middle-of-the-road SSP2-4.5 GHG scenario. Only six ESMs performed the G6sulfur simulations, either prescribing aerosol
properties scaled from earlier model experiments or deriving the aerosol distribution interactively from SO_2 gas injections
30   (Visioni et al., 2021b). Of these six models, only three included interactive stratospheric chemistry, and only two included
comprehensive aerosol microphysical processes. The resulting aerosol distributions and surface area density (SAD) strongly
differed in structure, location, and magnitude. Consequently, these differences led to different chemical processing and radiative
heating responses that impact transport and ozone (Tilmes et al., 2022). Furthermore, besides the relative large-scale cooling
from SAI, simulated regional changes in surface climate are a result of the influence of stratospheric changes or induced by
35   the residual feedbacks from the ocean or land surface (Banerjee et al., 2021; Wunderlin et al., 2024; Bednarz et al., 2023).
Due to the range of factors contributing to the simulated SAI responses, it has been challenging to determine the reasons for
inter-model differences.

Here, we describe a simplified SAI experiment for models participating in the second phase of the Chemistry-Climate
Modeling Initiative (CCMI-2022). CCMI is a follow-up project on the Chemistry Climate Model Validation (CCMVal and
40   CCMVal2) activity. The CCMVal simulations were used for multi-model assessment of a range of stratosphere-related pro-
cesses, most importantly in support of the earlier Ozone Assessment Reports (WMO, 2007, 2010), as well as used to produce
a comprehensive assessment report on chemistry-climate model evaluation and performance (Eyring et al., 2010). These as-
sessments evaluated a large number of models focusing on various chemical, dynamical, and radiative processes relevant to
simulating stratospheric ozone. CCMI expanded the scope of the project to both tropospheric and stratospheric processes.
45   The latest set of CCMI-2022 experiments was defined by Plummer and Co-authors (2021). State-of-the-art chemistry-climate
models with interactive chemistry participated in CCMVal and CCMI experiments and performed reasonably well regarding
the historical and future evolution of stratospheric species, including ozone (e.g., Keeble et al., 2021). In CCMI-2022, most
models included an interactive ocean to perform future experiments, although models without that capability can prescribe
sea-surface temperatures (SSTs) and sea ice from other models. All these models are required to provide historical 1960 –
50   2018 reference simulations, called refD1, and future CCMI reference simulations, based on a specific future scenario called
refD2 (Plummer and Co-authors, 2021).

For the SAI experiment described here, called senD2-sai, the stratospheric aerosol distribution or optical properties (ex-
tinction coefficients, single scattering albedo, and asymmetry factors of sulfuric acid aerosols) are prescribed based on a pre-

existing aerosol distribution obtained from a fully interactive simulation. In addition, each model uses fixed climatological

55 sea-surface temperatures and sea ice derived from its own refD2 simulations over the control period (2020 – 2030) to mini-
mize changes in global surface temperatures while land surface temperatures are still interactive. Such experimental design has
several benefits. First, it allows us to remove the uncertainty arising from the model representation of aerosol microphysical
processes and, hence, to identify inter-model differences in the stratospheric chemistry and circulation response to SAI under
the same aerosol perturbation. Second, the prescribed SST and sea ice conditions remove the influence of model-to-model

60 differences in climate sensitivity that would require different injection amounts in an interactive setting. Third, by removing
feedbacks from the ocean and cryosphere, this experimental setup allows us to isolate the stratospheric (top-down) impact of
SAI on the troposphere and removes any potential (bottom-up) influences from an uncertain ocean response. Finally, the model
setup allows more modeling groups that don't include comprehensive aerosol microphysics or ocean coupling to participate in
SAI experiments.

65   In the first part of this paper, we describe the experimental setup of senD2-sai and detail the procedure behind the production
of the aerosol properties to be prescribed by models. The second part compares the results of the fully coupled CESM2
(WACCM6) SAI simulations with interactive aerosols and ocean and the analogous senD2-sai experiment with prescribed
stratospheric aerosols and fixed SSTs and sea ice.

2   Model Description and Experimental Design

70 2.1   Model Description

We use the Whole Atmosphere Community Climate Model version 6 (WACCM6), a configuration of the Community Earth
System Model version 2 (CESM2) (Danabasoglu et al., 2020), to perform the experiments described below and summarized
in Table 1. The atmospheric model includes comprehensive chemistry in the troposphere, stratosphere, mesosphere, and lower
thermosphere (TSMLT) (Gettelman et al., 2019; Emmons et al., 2020). CESM2 (WACCM6), called WACCM6 in the follow-

75 ing, includes a prognostic representation of tropospheric and stratospheric aerosols using Modal Aerosol Microphysics version
4 (MAM4) (Liu et al., 2016) and sulfur emissions from volcanoes and other sources (Mills et al., 2017). The model is coupled
to the Community Land Model version 5 (CLM5) (Lawrence et al., 2019) and the Parallel Ocean Program version 2 POP2
(Danabasoglu et al., 2020). Different model configurations allow it to be run with a prescribed stratospheric aerosol distribu-
tion and sea surface temperatures (SSTs) and sea ice, as required for the senD2-sai experiment.

80 2.2   Climate change simulations (SSP2-4.5 and refD2)

SSP2-4.5 is the middle-of-the-road CMIP6 scenario (Meinshausen et al., 2017) and the CESM2 simulations were started in
2015 from the historical free-running simulations (Gettelman et al., 2019). The continuous increase in GHG concentration
in SSP2-4.5 results in an increase in near-surface air temperature of around 2°C and precipitation of 0.12 mm/day by the
end of the 21st century, compared to 2020 – 2030 conditions (Figure 1, top and panel, green lines). For producing elevated

85   stratospheric background aerosol conditions to represent eruptive volcanoes, the experiment used an average of the eruptive volcanic SO_2 emissions from 1850 to 2015, following the recommended CMIP6 setup for preindustrial control and future conditions (Danabasoglu et al., 2020). The simulated stratospheric AOD (SAOD) at 525 nm wavelength in the model agrees well with observations from the Global Space-based Stratospheric Aerosol Climatology (GloSSAC) for stratosphere aerosol properties (Thomason et al., 2018) and remains higher than volcanically clean observed periods (Figure 1, bottom).

90   In WACCM6, the eruptive stratospheric volcano emissions between 2015 and 2025 were implemented slightly differently in SSP2.4-5 than in refD2, resulting in different stratospheric AOD (Figure 1, bottom). In refD2, eruptive sulfur injections transitioned from the current state in 2015 towards elevated background emissions described above within the first ten years (Plummer and Co-authors, 2021), while in SSP2-4.5 these elevated emissions were implemented abruptly in 2015. The resulting lower SAOD in refD2 between 2015 and 2025 than the SSP2-4.5 experiment (Figure 1, bottom) is expected to result

95 in differences in the climate response between SSP2-4.5 and refD2 in the first ten years of the experiment using WACCM6. However, global near-surface temperature and precipitation differences are insignificant between the experiments, given the variability of global surface temperature and total precipitation (Figure 1, top and middle panels, blue and red lines).

    The CCMI-2022 future refD2 scenario uses GHG and aerosol forcings similar to the SSP2-4.5 experiment. However, the experiment uses the baseline scenario from WMO (2018) for halogenated ozone-depleting substances (ODS) that include small

100 changes to the assumed future surface concentrations of ODS compared to those used in SSP2-4.5 (Plummer and Co-authors, 2021), leading to approximately 10% higher future (2080 -– 2099) stratospheric halogen (Cly and Bry) levels in refD2 compared to SSP2-4.5 (Figure S1). The larger halogen levels in refD2 are expected to lead to differences when comparing the stratospheric ozone between refD2 and SSP2-4.5.

2.3   Interactive SAI simulation (SSP2-4.5 SAI)

105 The SSP2.4-5 SAI experiment produces the aerosol distribution input for senD2-sai and is based on the SSP2.4-5 setup using WACCM6, described above. When this experiment was performed, the refD2 experiment was unavailable, which would have been a more consistent control experiment than SSP2.4-5. However, despite small differences in future forcings, this experiment is expected to produce a similar stratospheric aerosol distribution. The experiment starts in 2020 from the corresponding SSP2.4-5 simulation, including CMIP6 GHGs and ODS, and elevated eruptive volcanic emissions described above. The in-

110 jections of SO_2 start in 2025, five years after the start of the experiment to keep near-surface temperatures at 2020 — 2030 (inclusive) average conditions of the corresponding SSP2.4-5 simulation.

    To achieve these temperature targets, we are using a similar setup as in previous SAI studies using WACCM6 (e.g., Tilmes et al., 2018a; Tilmes et al., 2022; Richter et al., 2022; Bednarz et al., 2023; Zhang et al., 2024b). In detail, WACCM6 incorporates a feedback control algorithm (MacMartin et al., 2017) which controls the injection of SO_2 at four point locations,

115 here at 15°N, 15°S and 30°N, 30°S, in all cases at 180°W in longitude and about 1 km above the tropopause in altitude (so 19.2-19.4 km at 15°N and S, and 18-18.2 km at 30°N and S). Previous studies targeted three climate goals (with three degrees of freedom) to maintain global mean surface temperatures and their interhemispheric and equator-to-pole gradients at predefined levels (e.g., Kravitz et al., 2017). In SSP2-4.5 SAI, we modified the existing feedback control algorithm to require
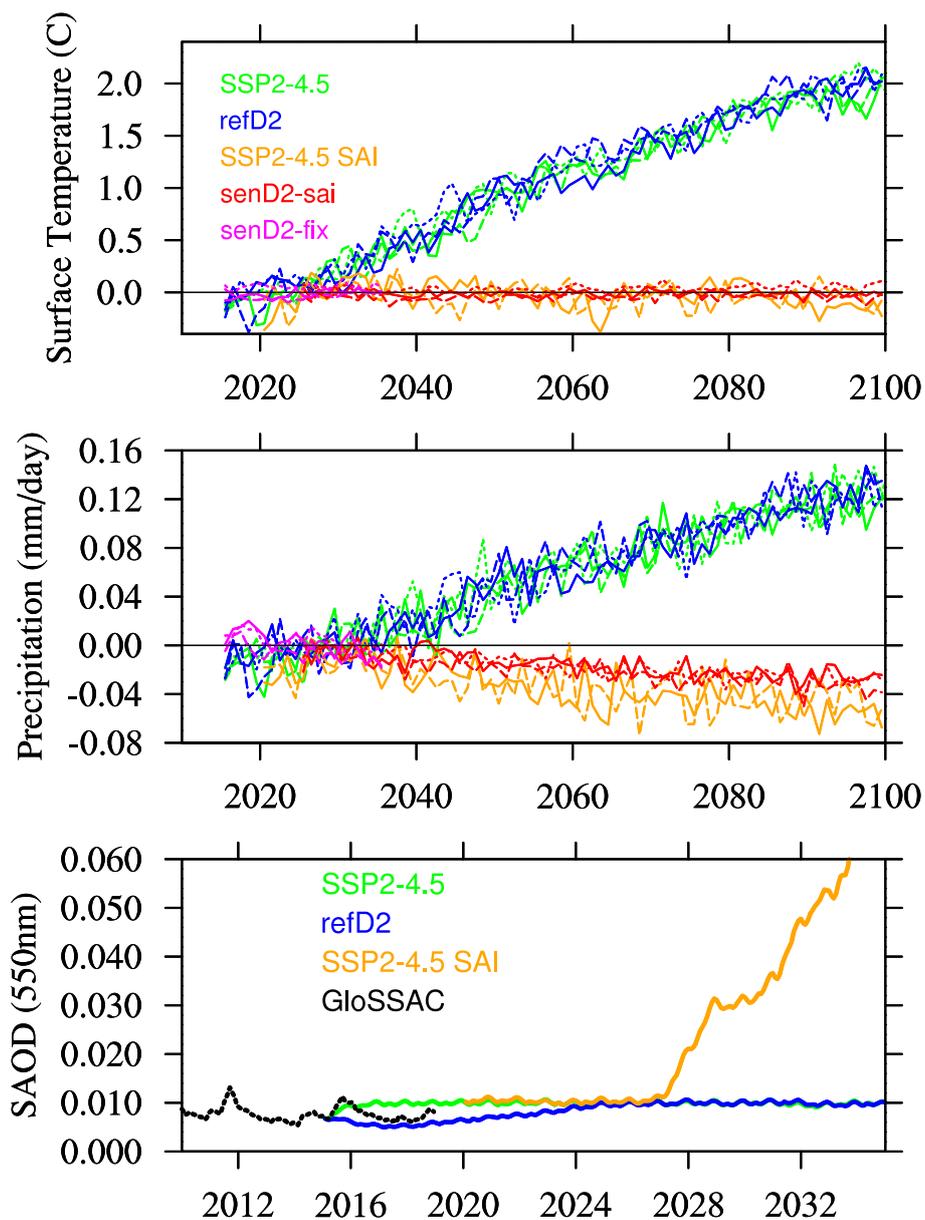
Figure 1. Changes in global mean air surface temperatures (top), precipitation (middle), and stratospheric aerosol optical depth averaged between 80°N and 80°S (consistent with GloSSAC observations (bottom panel) compared to 2020 – 2030 average conditions, for different experiments performed with CESM2(WACCM6).
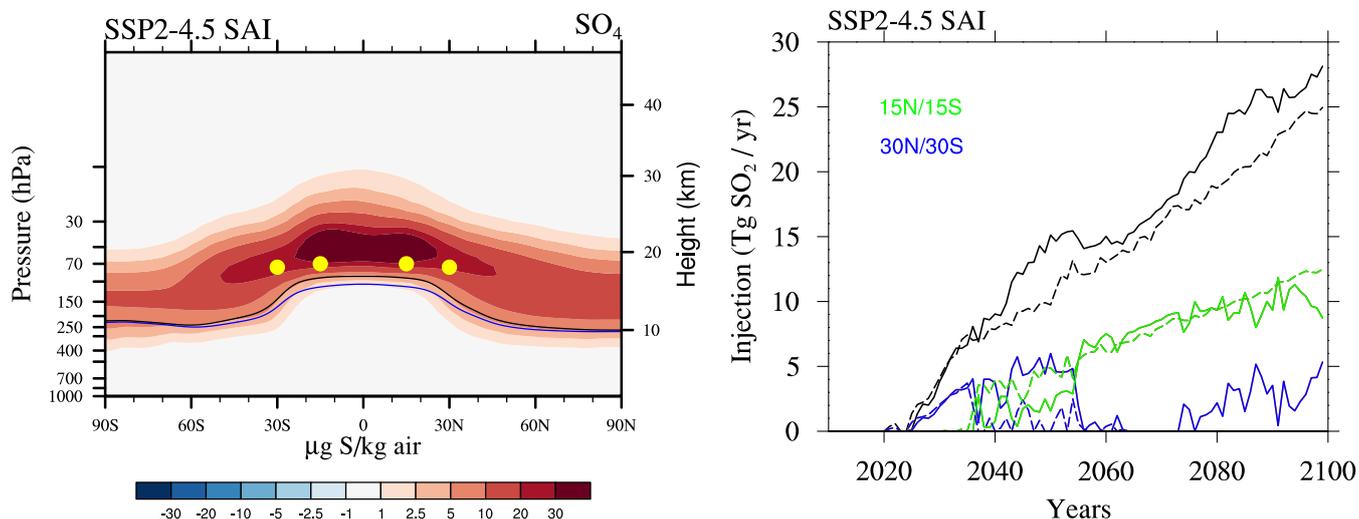
Figure 2. Left panel: Differences of zonally and annually averaged SO_4 concentrations between the SSP2-4.5 SAI experiment in 2080 – 2099 and the control experiment (SSP2-4.5) in 2020 – 2030. The lapse rate tropopause is indicated as a black line for the control experiment and a blue line for the SO_2 injection cases. Yellow dots are the locations of injection. Right panel, annual injection rates of SO_2 at $15°$N and $15°$S (green lines), at $30°$N and $15°$S (blue line), and the total (black lines). Different lines indicate the result of two different ensemble members.

that sulfur injections are equally distributed into both hemispheres to maintain the global near-surface temperature and the
120   equator-to-pole at the desired level (Figure 1, top for near-surface temperature).

The modified choice of climate targets compared to the previous WACCM6 SAI studies is to produce a symmetric strato-
spheric aerosol distribution and SAOD in the two hemispheres, requiring more SO_2 injections at $15°$N and S and $30°$N and S
(Figure 2). Previous studies with three degrees of freedom for SO_2 injections show that more injections are often required in
one hemisphere to keep the interhemispheric temperature gradient from changing. The details are strongly model-dependent
125   and due to differences in internal feedbacks and sensitivities to increasing GHGs and SAI (e.g., Fasullo and Richter, 2023;
Henry et al., 2023). However, differences in the interhemispheric aerosol distribution lead to different chemical (ozone) and
dynamical responses and are not desired for multi-model comparisons.

2.4   CCMI-2022 senD2-sai and senD2-fix simulations

The CCMI senD2-sai experiment is designed to keep global mean surface temperatures from changing from 2020 – 2030
130   conditions while greenhouse gas concentrations, ODS, and emissions follow the refD2 CCMI future model experiment (see
Figure 1, top panel, red lines). However, instead of including interactive stratospheric aerosols through stratospheric SO_2
injections, it uses the stratospheric aerosol distribution or aerosol properties provided by the SSP2-4.5 SAI experiment starting
in 2020. The information provided by WACCM6 results for the CCMI experiment includes 5-day instantaneous zonal mean
output of sulfate aerosol concentrations for the three available aerosol modes, surface area density in both the troposphere and

135 stratosphere, effective radius, and aerosol optical depth at 500 nm between 2020 and 2100. Since some CCMI-2022 models require additional information on aerosol properties available from WACCM6, this data is further complemented with the data described in Section 2.5 below.

For WACCM6 senD2-sai, the 5-day instantaneous varying stratospheric aerosol distribution can be directly used. For chemical processing, WACCM6 uses the prescribed aerosol surface area density (SAD) (called SAD-AERO) from SSP2-4.5 SAI.

140 This variable ignores the swelling and uptake of nitric acid and water vapor for cooler temperatures below 200 K and only assumes liquid binary solutions. For chemical heterogeneous reactions in the stratosphere, WACCM6 then internally calculates another aerosol SAD variable (called SAD-SULFC) that considers both liquid binary sulfate aerosols and supercooled ternary solutions, as well as two additional SAD variables for polar stratospheric clouds (Kinnison et al., 2007; Solomon et al., 2015). For radiative calculations, WACCM6 uses the 5-day zonal mean mass and wet radius of the three stratospheric aerosol modes

145 from the SSP2-4.5-SAI simulation to derive radiative properties.

In addition, for senD2-sai, instead of using an interactive ocean, climatological SSTs, and sea ice values are prescribed using the model-specific 2020 – 2030 (inclusive) climatology of the corresponding refD2 experiment throughout the senD2-sai simulation length. The prescribed SSTs, therefore, match the SAI temperature target. As a result, only minor global mean surface temperature variations are simulated in senD2-sai due to changes from the atmosphere and land (Figure 1, red lines,

150 top panel). On the other hand, the feedback from the atmosphere and land changes in the globally averaged precipitation in senD2-sai is similar to that in SSP2-4.5 SAI (Figure 1, red lines, middle panel). Details of the difference in surface climate between these two experiments will be discussed in Section 3.

While SAI starts in 2025 in senD2-sai, we recommend that models start their simulations in 2020 to adjust to the new background aerosol distribution (see Section 2.2). This is desirable since not all models use the same aerosol background

155 conditions for refD2. We further require performing a background aerosol experiment senD2-fix. This experiment is identical to senD2-sai; however, instead of using the time-varying prescribed stratospheric aerosol described above, this experiment repeats background climatological stratospheric aerosol averaged between 2020 – 2024 (inclusive). This simulation is required to be performed over 2015 – 2035 (pink lines in Figure 1) at the least, but it is recommended that it be extended until the end of the century if possible.

160 **2.5 Prescribed aerosol properties**

The provided stratospheric aerosol distribution from the WACCM6 SSP2-4.5 SAI simulation does not contain sufficient information, particularly the optical properties extinction coefficient, single-scattering albedo, and asymmetry factor at all the different wavelengths, needed for some CCMI-2022 models. Optical properties for all required wavelengths have not been provided from WACCM6. To produce this information, Jörimann et al. (2024) developed a method to produce the required

165 aerosol and optical properties from the provided WACCM6 distribution. In detail, the number density (called: NUM-A[1-3]) and wet diameter (called: DGNUMWET[1–3]), as well as a fixed half-width σ were used to characterize the size distribution of the three aerosol modes. The half-widths are 1.6, 1.6, and 1.2 for the three modes, respectively. Model output temperature and relative humidity fields were used to calculate the water weight percentage of the aerosol particles. With these parameters

being known, all three optical properties can readily be calculated and summed up over the three modes using Mie theory for a
170 homogeneous sphere (Bohren and Huffman, 1998), i.e., a liquid aerosol particle. With this method, the optical properties can
be given for any wavelength band, making it adaptable to any radiation scheme spectral resolution.

3 Prescribed aerosols versus interactive injections

Using WACCM6, we can directly compare the fully interactive SSP2-4.5 SAI experiment results with the senD2-sai simulation
with prescribed stratospheric aerosol and fixed SSTs and sea ice in the same model framework. Differences between the
175 two experiments are only due to the experimental setup discussed above, while information from the derived stratospheric
aerosol distribution, namely surface area density (SAD), aerosol mass, and mode radius provided from SSP2-4.5 SAI, are
adopted without any required adjustments, described in Section 2.5. In the following, we compare the results of these two SAI
experiments, SSP2-4.5 SAI and senD2-sai, for the future 2080 – 2099 period against their respective control simulation from
SSP2-4.5 and senD2-fix, respectively, for the period 2020 – 2030, see Table 1).

180 ### 3.1 Stratospheric chemistry and dynamics response to SAI

The effects of SAI on stratospheric temperature, dynamics, and chemistry across multiple models have been discussed in
previous papers (e.g., Niemeier et al., 2020; Visioni et al., 2021a; Tilmes et al., 2022; Bednarz et al., 2023), and are briefly
reviewed below. Here, we mainly focus on the differences between the fully interactive model experiment and those using
prescribed stratospheric aerosol and SSTs and sea ice.

185 By construction, SAD-AERO simulated in SSP2-4.5 SAI and prescribed in refD2-sai are similar in the stratosphere (as
shown in Figure 3 top row, described in Section 2.4), with slightly smaller values in the extratropical lower stratosphere in
SSP2-4.5 SAI. In the interactive aerosol simulation, SAD is calculated for each grid point, while SAD in the prescribed exper-
iment uses zonal mean values, likely leading to slight differences. Furthermore, in the interactive stratospheric aerosol simu-
lation, aerosols are transported and sediment into the troposphere and deposited at the surface. In contrast, for the prescribed
190 stratospheric aerosol experiment, the model zeros out the prescribed aerosol distribution and SAD below the troposphere. In
WACCM6, the tropopause is internally calculated via the WMO lapse rate calculation for latitudes lower than 50°N and S. It
uses climatological tropopause values for latitudes larger than 50°N and S due to difficulties deriving the tropopause at all times
in higher latitudes, which is generally lower than the model internal tropopause. Therefore, the prescribed SAD in senD2-sai
reaches lower vertical levels than indicated by the internally calculated tropopause in Figure 3 blue and black lines (top middle
195 plots). The small differences in SAD-AERO in the troposphere and stratosphere are not expected to largely impact strato-
spheric heterogeneous chemistry. Furthermore, corresponding differences in aerosol mass could result in small differences in
the radiative response, as discussed below.

Changes in temperature and other variables result from the increasing GHG concentration and changes in ODS levels be-
tween 2080 – 2099 and 2020 – 2030, and SAI. The strong decrease in temperature in the upper stratosphere for both SAI
200 experiments compared to the control results from higher GHGs in 2080 – 2099 compared to 2020 – 2030 (Figure 3, second
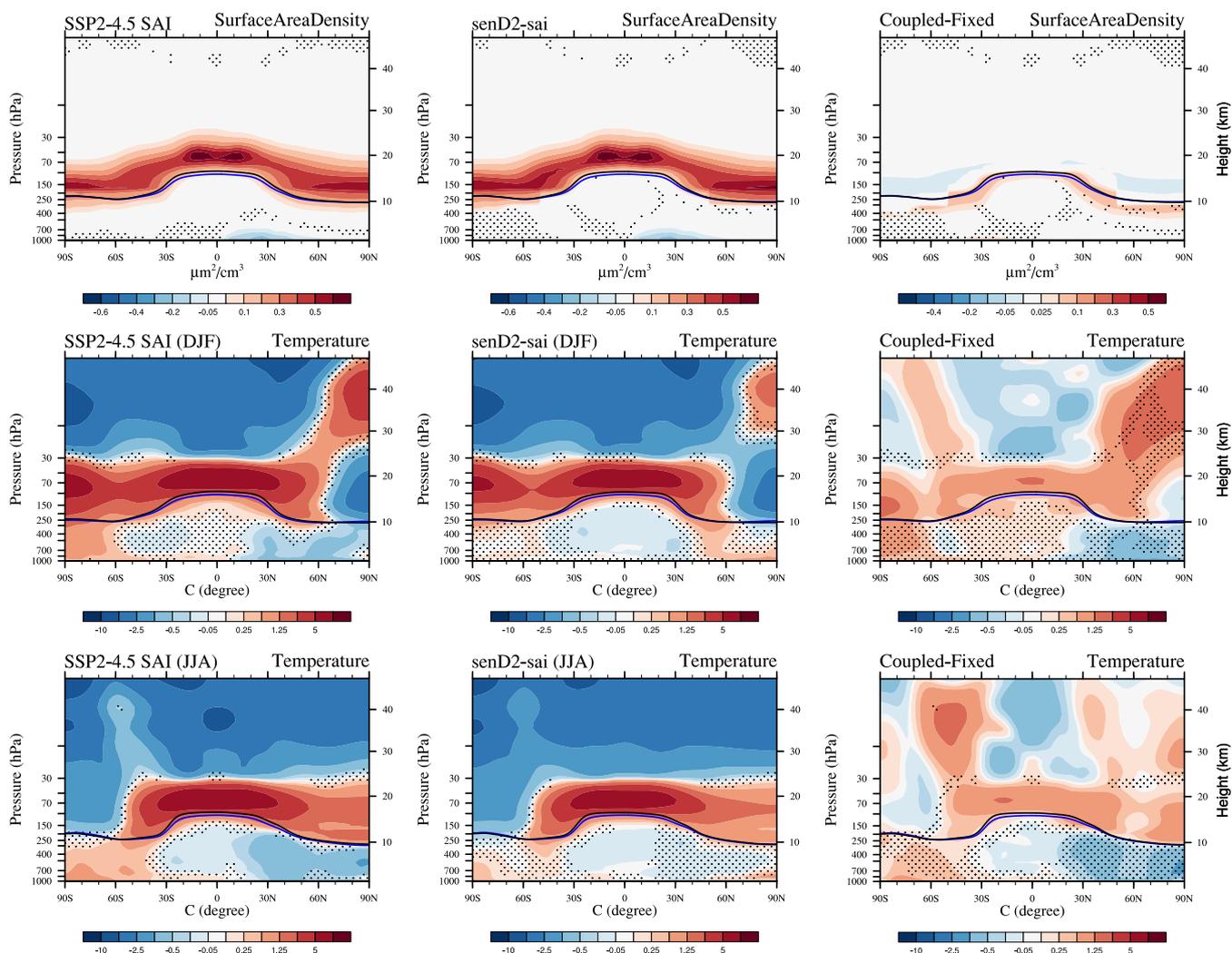
Figure 3. Top row: Differences of zonally and annually averaged Surface Area Density (SAD-AERO, see text for more detail) between SSP2-4.5 SAI in 2080 – 2099 and the control experiment (SSP2-4.5) in 2020 – 2030 (left); between senD2-sai and the control experiment (senD2-bg) in 2020 – 2030 (middle); and between SSP2-4.5 SAI and senD2-sai in 2080 – 2099 (right). Middle and bottom row: Differences of zonally averaged temperature for December/January/February (middle row) and June/July/August (bottom row), between SSP2-4.5 SAI in 2080 – 2099 and the control experiment (SSP2-4.5) in 2020 – 2030 (left); between senD2-sai and the control experiment (senD2-bg) in 2020 – 2030 (middle); and between SSP2-4.5 SAI and senD2-sai in 2080 – 2099 (right). The lapse rate tropopause is indicated as a black line for the control experiment and a blue line for the SAI cases (left and middle panels). Areas of non-significant difference at the 95th % level to the control are marked as small black dots.
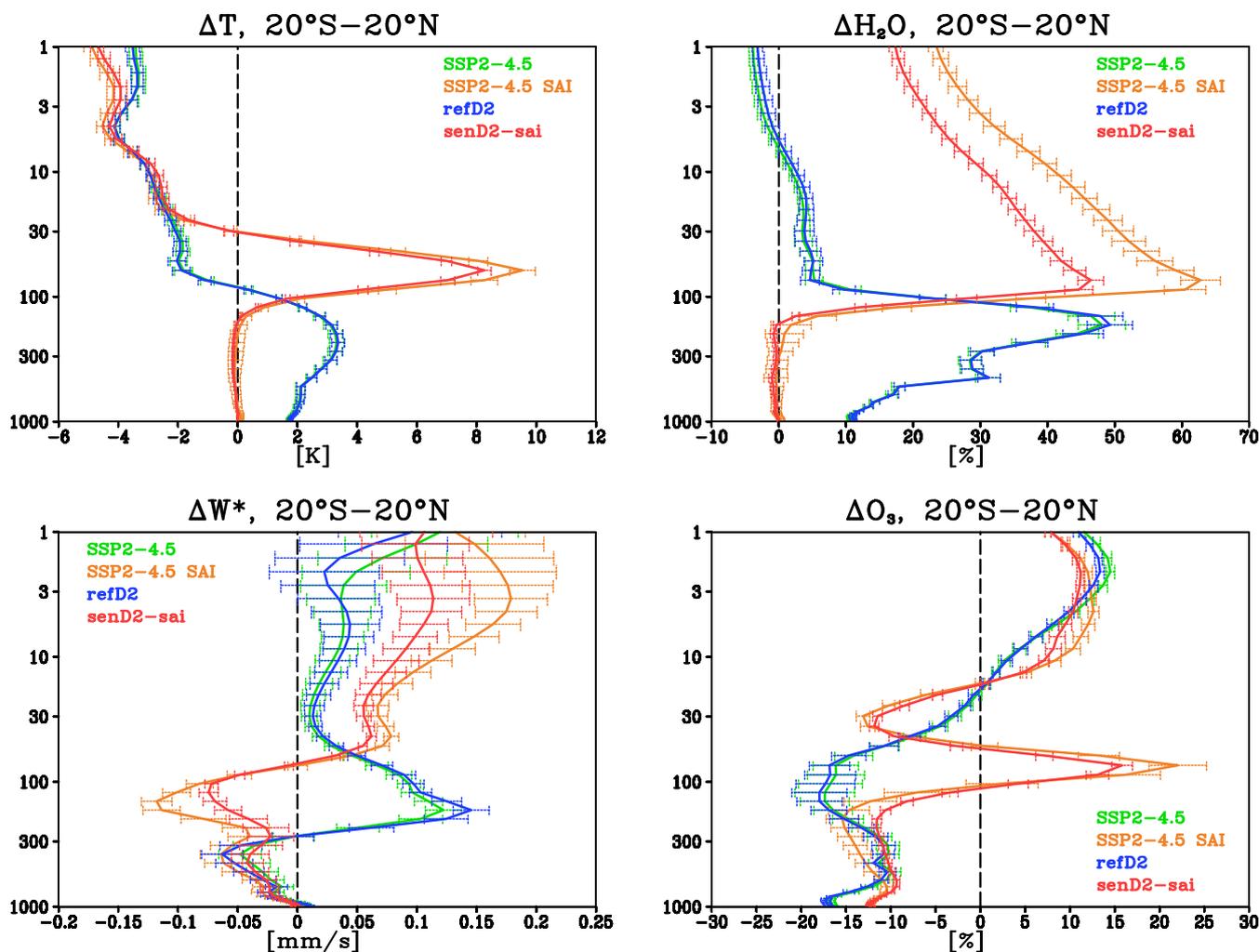
Figure 4. Zonal mean differences between $20°N$ and $20°S$ between $2080 - 2099$ and control conditions ($2020 - 2030$), for temperature (top left), water vapor (top right), transformed Eulerian mean vertical velocity ($w^\star$) (bottom left), ozone (bottom right), for the different experiments.

and third row, left and middle panels). On the other hand, SAI increases temperatures in the tropical lower stratosphere by 5-10 K and in the summer polar lower stratosphere by 2-5 K, mainly due to the absorption of long and short-wave radiation from the elevated sulfate mass (Figure 3, middle and bottom row; Figure 4, left panel). The resulting increase in tropical tropopause temperatures significantly increases water vapor in the stratosphere (Figure 4, second panel), which counters some of the sur-

205   face cooling effects of SAI. Increasing stratospheric water vapor with SAI also impacts stratospheric chemistry via changes in the reactive hydrogen ozone-destroying cycle (e.g., Tilmes et al., 2018b; Bednarz et al., 2023; Wunderlin et al., 2024).

Comparisons between senD2-sai and SSP2-4.5 SAI compared to the control show stronger warming of up to 1 K in SSP2-4.5 SAI in the lower tropical stratosphere. The stronger warming around and slightly below the tropopause in SSP2-4.5 SAI is consistent with a larger sulfate mass near the tropical tropopause, as discussed above. However, the stronger warming in SSP2-4.5 SAI compared to senD2-sai around 70 hPa (Figure 3, right panels) cannot be explained by the small differences in the aerosol mass, since aerosol heating shows a local response (Richter et al., 2017). In contrast, the simulated stronger temperature increase in the coupled vs. the constrained experiment is more likely related to the stronger concurrent coupling with the dynamical changes, in particular the tropical upwelling (as illustrated by the vertical component, of the Transformed Eulerian Mean (TEM) circulation, $w^\star$), as well as related changes in ozone in this region (Figure 4), as explained in the following.

SAI impacts the BDC (driven by wave forcing described by the TEM), primarily because of the aerosol-induced lower stratospheric heating and reduction incoming solar radiation impacting atmospheric static stability in both the troposphere and stratosphere, as well as changing zonal winds, which modulate planetary wave propagation and breaking (e.g., Tilmes et al., 2018b; Bednarz et al., 2023). The result is a weakening of the tropical upwelling in the upper troposphere and lower stratosphere and the associated weakening of the shallow branch of the BDC (Figure 4, panel 3). The increase in the upwelling in the mid-to-upper stratosphere above the sulfur injection location, on the other hand, is indicative of an acceleration of the deep branch of the BDC. In SSP2-4.5 SAI, the slightly stronger warming in the tropical lower stratosphere compared to senD2-sai is also consistent with a stronger weakening of the tropical upwelling below the SAI injection location. This is indicative of a generally stronger response in the interactive aerosol simulation than in those with prescribed aerosols. In addition, the reduced upwelling results in reduced tropospheric ozone-poor air entering the lower stratosphere, resulting in more ozone and therefore more heating, which amplifies the heating differences between SSP2-4.5 SAI and senD2-sai. The difference in upwelling between the two experiments may be caused initially by the slightly warmer temperatures around the tropopause (due to more aerosol mass) in the interactive model run.

The simulated temperature reductions in the winter polar lower stratosphere are also impacted by dynamical changes, namely a stronger polar vortex under SAI (e.g., Tilmes et al., 2022), shown for both Arctic and Antarctic polar vortices (Figure 5). The simulated weakening of zonal winds in the Antarctic stratosphere in austral summer (DJF) (Figure 5, top), also contributes to the direct radiative changes from aerosol absorption discussed above, amplifying the warming simulated in the Antarctic lower stratosphere in DJF. In addition, increased GHG and decreased ODS levels (comparing future vs present-day conditions) likely contribute to the simulated strengthening of the polar vortex shown in Figure 5 (WMO, 2022, and references therein), (Butchart et al., 2010; McLandress et al., 2010; Karpechko et al., 2022). Temperature differences between SSP2-4.5 SAI and senD2-sai in high latitudes are small, with a somewhat weaker polar vortex in both hemispheres polewards of sixty degrees in the interactive SSP2-4.5 SAI simulation. This may be in part a result of ocean coupling countering the stronger surface pressure reduction simulated over the winter pole in senD2-sai, discussed below.

Changes in high latitudes are further coupled to large-scale changes in the BDC. ESMs project future speeding up of the BDC under global warming as the result of GHG-induced changes in surface and atmospheric temperatures impacting wave generation, propagation, and breaking (e.g., Butchart et al., 2010; Hardiman et al., 2014; Abalos et al., 2021; Keeble et al.,
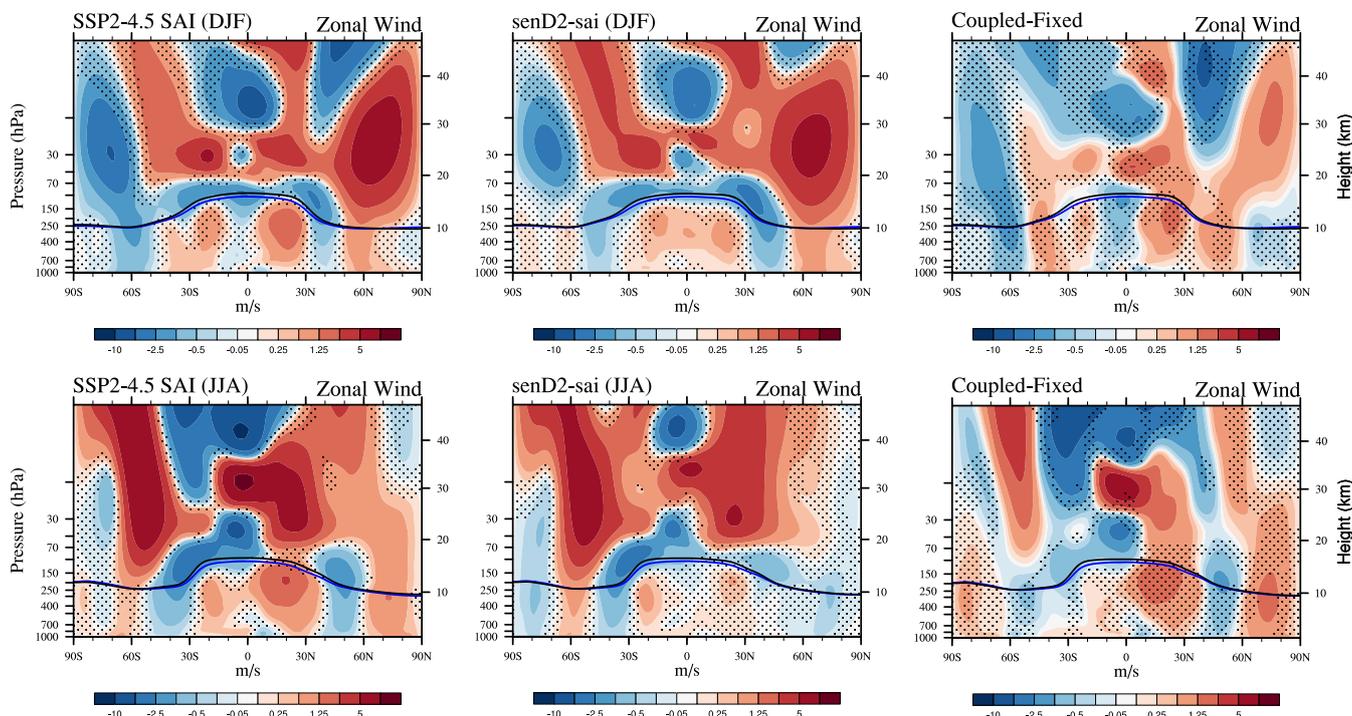
Figure 5. Differences of zonally averaged zonal wind velocity for December/January/February (top row) and June/July/August (bottom row), between SSP2-4.5 SAI in 2080 – 2099 and the control experiment (SSP2-4.5) in 2020 – 2030 (left); between senD2-sai and the control experiment (senD2-bg) in 2020 – 2030 (middle); and between SSP2-4.5 SAI and senD2-sai in 2080 – 2099 (right). The lapse rate tropopause is indicated as a black line for the control experiment and a blue line for the SAI cases (left and middle panels). Areas of non-significant difference at the 95th % level to the control are marked as small black dots.

2021). The stronger increase in $w^\star$ in the stratosphere above the injection locations in SSP2.4-5 SAI is aligned with the stronger heating in the tropical lower stratosphre compared to senD2-sai, and it coupld be further caused by increased wave-driven changes initiated in the troposphere. Furthermore, SSP2.45 SAI shows stronger zonal mean wind changes in the tropical

245 troposphere, most pronounced in the NH. The weakening of the subtropical tropospheric jet (STJ) is reaching all the way down to the surface in SSP2.45 in both hemispheres, while the response is much weaker in senD2-sai, in particular for the NH. These differences point to the importance of ocean feedback in SSP2-4.5 SAI, while some differences may also result from the differences in near-surface temperature response in the two experiments, as further discussed in Section 3.2.

The simulated changes in stratospheric ozone between 2080–99 and 2020–30 in the SAI runs, as shown in Figure 6, are

250 due to the combined effects of increasing GHGs, decreasing stratospheric halogen levels, and SAI forcings. The direct effect of SAI on ozone is illustrated in Figure S2, comparing SSP2-4.5 SAI minus SSP2-4.5 and senD2-sai minus senD2-fix for future conditions. The interplay of chemical vs dynamical drivers of ozone depends on location and season (e.g., WMO, 2022). Compared to the present day and independent of SAI, the most pronounced changes in ozone mixing ratios in future scenarios
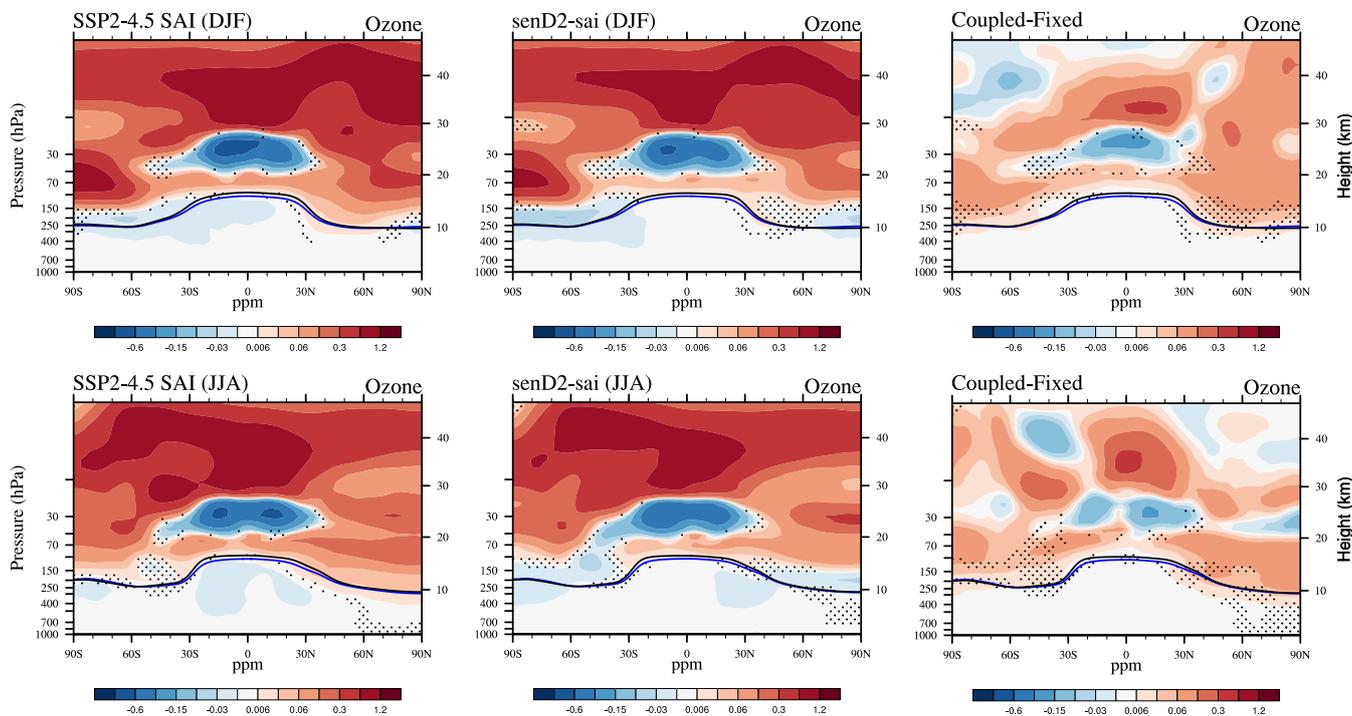
Figure 6. Differences of zonally averaged ozone mixing ratios (ppm) for December/January/February (top row) and June/July/August (bottom row), between SSP2-4.5 SAI in 2080 – 2099 and the control experiment (SSP2-4.5) in 2020 – 2030 (left); between senD2-sai and the control experiment (senD2-bg) in 2020 – 2030 (middle); and between SSP2-4.5 SAI and senD2-sai in 2080 – 2099 (right). The lapse rate tropopause is indicated as a black line for the control experiment and a blue line for the SAI cases (left and middle panels). Areas of non-significant difference at the 95th % level to the control are marked as small black dots.

is the substantial increase in ozone concentration in both the upper stratosphere and the polar regions, dominated by reduced
255 halogen content in 2080 – 2099 compared to 2020 – 2030. In addition, the increase in GHG concentrations results in a cooling of the upper stratosphere and, consequently, a slowing of reactive ozone-depleting cycles (Haigh and Pyle, 1982). Furthermore, adding SAI increases ozone in the mid-to-upper stratosphere due to increased nitrogen pentoxide hydrolysis, reducing nitrogen oxide and the resulting catalytic ozone loss. The decrease in ozone in the middle tropical stratosphere at ≈30 hPa and increases in the lower tropical stratosphere are, for the most part, dynamically driven by the acceleration of the tropical upwelling above
260 the SAI injection location and the enhanced transport of lower ozone concentrations into this region, as well as the reduced upwelling below SAI injections with reduced transport of ozone poor tropospheric air masses above the tropopause region, as discussed above (Figure 4, third and fourth panel). In addition, enhanced stratospheric water vapor due to the warming of the tropical tropopause increases the reactive hydrogen ozone loss cycle. Finally, reductions in ozone in the SH polar lower stratosphere with SAI are the result of increased heterogeneous reactions with increased SAD and a stronger polar vortex
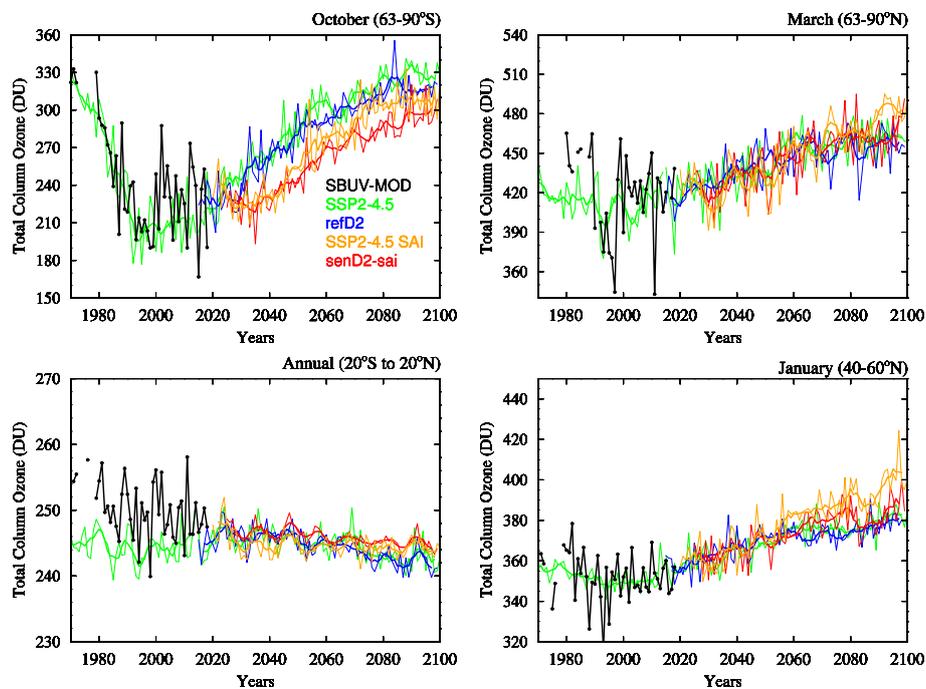
Figure 7. Ensemble mean total column ozone for October between 63-90°S (top left), March between 63-90°N (top right), annual average between 20°S-20°N (bottom left), and January between 40-60°N (bottom right) for different model experiments. Total column ozone observations from the Solar Backscatter Ultraviolet (SBUV) Merged Ozone Data (MOD) set (Frith et al., 2017) are shown as black lines.

265 (Figure S2), which is countered by the increase in ozone due to reductions in stratospheric halogen burden under decreasing ODS levels as well as due to the SAI-induced changes in ozone transport and BDC compared to present day (WMO 2022).

Direct SAI-induced changes differ slightly between senD2-sai and SSP2-4.5 SAI (Figure 6, right panels, Figure S2). Comparison between changes in SSP2-4.5 SAI and senD2-sai reveal larger magnitudes of the tropical ozone anomalies, in particular, a stronger increase of ozone above the tropical tropopause in the coupled runs, in accord with the concurrent stronger lower

270 stratospheric heating and changes in tropical upwelling discussed above. Significant differences between SSP2-4.5 SAI and senD2-sai also occur in the polar regions, including more pronounced reductions of SH polar ozone in senD2-sai. Differences in the polar lower stratospheric ozone anomalies between the coupled and constrained simulation could also be related to slightly lower aerosol SAD changes in the coupled run (Figure 3, top row), which reduces the amount of halogen activation and chemical ozone loss. In addition, higher polar ozone concentrations in SP2-4.5 SAI are aligned with the greater changes

275 in the SAI-induced BDC due to the stronger tropical stratospheric heating in the coupled run and wave-driven changes arising from ocean feedbacks. Resulting differences, particularly in polar ozone concentrations, affect the evolution of Total Column Ozone (TCO) after 2060 (Figure 7).

In summary, the stratospheric ozone response to SAI in the prescribed vs interactive (fully-coupled) aerosol simulation is overall similar. Minor differences in the responses for the different model setups in TCO in the future are expected due to

280 differences in the ODS between SSP2-4.5 and refD2, resulting in larger values in SSP2-4.5 for the SH winter polar region (Figure 7, left top panel). Differences in the SAI-induced changes are due to the stronger tropical lower stratospheric heating and the resulting impacts on zonal winds and BDC in a coupled simulation. In addition, climate feedbacks resulting from the coupling to SSTs and sea ice in SSP2-4.5 SAI affect dynamical changes in the stratosphere, including enhanced induced wave activities in the troposphere that strengthen the BDC and weaken the polar vortex. These changes may be in part driven by

285 the El-Nino like response in the tropical Pacific and its teleconnections, as well as uneven near-surface temperature changes in the coupled simulation. These combined differences result in a slightly larger TCO in the SH polar ozone hole and a slightly smaller SAI-induced reduction in TCO in the interactive simulation. However, by the end of the experiment, SAI-induced changes in both SSP2-4.5 SAI and senD2-sai are around 10-20 DU after 2070 (Figure 7, left top panel). In the NH winter polar region, the increase in TCO is consistent in all four simulations, with a slightly larger increase of TCO in SSP2-4.5 SAI

290 after 2080, consistent with the stronger wave activity in that run (Figure 7, right top panel). Similarly, TCO shows a stronger increase in the interactive simulation in January NH mid-latitudes reaching up to 10 DU (Figure 7, right bottom panel). In the tropics, the slight SAI-induced increase in TCO of around 3 DU by the end of the simulation is consistent for both experiments and counters some of the TCO decline in the future without SAI (Figure 7, left bottom panel). Since the discussed differences between the prescribed and interactive experiment are similar, senD2-sai is expected to be suited to study the effects of SAI on

295 stratospheric chemistry and dynamics for multi-model comparison studies. However, the missing feedback from ocean and sea ice in senD2-sai leads to an underestimation of the dynamical response. This represents a caveat of using a less interactive set up to study the effects of SAI on ozone.

3.2 Tropospheric and surface climate response to SAI

In an interactive model simulation (SSP2-4.5 SAI), the feedback from the ocean plays a dominant role in the tropospheric

300 and surface climate response to SAI beyond the effects on stratospheric dynamics (discussed above). Differences between the surface climate response between SSP2-4.5 SAI and senD2-sai are analyzed in detail in the following. Changes in tropospheric and surface climate for hemispherically symmetric sulfur injections in WACCM6, including near-surface air temperature and precipitation patterns, have been discussed in detail by Zhang et al. (2024b); Bednarz et al. (2023). Here, we focus on regional differences between the fully coupled SSP2-4.5 SAI and prescribed senD2-sai simulations to isolate the contributions of the

305 dynamical influence via the stratosphere induced by the stratospheric aerosols and feedbacks induced by the coupling with the ocean.

In SSP2-4.5 SAI, mean global near-surface air temperatures have been successfully maintained at the levels corresponding to the target 2020 – 2030 climate (Figure 1 top panel). However, the experiment produces a significant overcooling in the Northern Hemisphere of up to 2°C in a zonal mean and a smaller residual warming of around 0.5°C in the Southern Hemisphere

310 high latitudes (Figure 8). The reason for the uneven cooling in CESM2 (WACCM6) under equal sulfur injections in both hemispheres with SAI (per design) is the model-specific sensitivity to elevated GHG concentrations and SAI. These include adjustments in the SH clouds and coupling with the Atlantic Meridional Overturning Circulation (AMOC), which have yet to be further explored (Fasullo and Richter, 2023). In contrast, the prescribed aerosol experiment, senD2-sai, successfully minimizes

changes in zonal mean near-surface air temperatures due to the use of the climatological SSTs and sea ice fixed to 2020 – 2030
315   conditions.

The SSP2-4.5 future climate scenario (Figure 9 left panels) and refD2 (not shown) regional temperature and precipitation changes look almost identical. Future scenarios without SAI show very strong increases in near-surface temperature and a significant reduction of surface temperatures in the North Atlantic region. This response has been discussed in different studies and is due to the projected decline in the strength of AMOC with increasing atmospheric GHG concentrations (e.g., Tilmes et al.,
320   2020; Zhang et al., 2024b; Li et al., 2023). SSP2-4.5 SAI shows a significant NH cooling (Figure 9, middle panel). The symmetric injection in both hemispheres using SAI has been shown to counter the weakening of the AMOC due to climate change in WACCM6 (Zhang et al., 2024b).

Significant relative warming occurs in the equatorial eastern Pacific in the SSP2-4.5 SAI experiment, similar to the El Nino pattern, and projects on a positive phase of the El Nino-Southern Oscillation (ENSO) (Trenberth, 2020). This response is
325   likely driven by the weakening of the Walker circulation (Bednarz et al., 2023) as a result of the increase in tropical stability due to the heating of the lowermost stratosphere that suppresses tropical convection (Simpson et al., 2019; Malik et al., 2020; Banerjee et al., 2021). However, the exact mechanisms driving this under SAI are yet to be explored (Rezaei et al., 2022). In general, changes in ENSO variability are important in modulating local climate in the tropical Pacific region and, via various teleconnections, can impact the atmosphere globally. For the northern Pacific, changes in the meridional temperature gradients
330   associated with the positive ENSO phase tend to strengthen the subtropical tropospheric jet, while increased tropospheric wave activity acts to deepen the Aleutian low pressure, influencing near-surface air temperature and precipitation patterns in western North America and north-east Asia (Domeisen et al., 2019); also Figure 9-10). The enhanced tropospheric wave activity under the positive ENSO phase can also enter the stratosphere, acting to strengthen BDC and weaken polar jets (discussed in Section 3.1). By design, the constrained senD2-sai experiment does not show any near-surface air temperature changes in the equatorial
335   Pacific and, thus, El-Nino-like teleconnections with tropospheric temperatures, winds, and surface pressure and precipitation patterns.

Differences of near-surface temperature in senD2-sai, Figure 9, right column, show a robust winter warming over Eurasia and cooling of North Atlantic and Greenland. In addition, some significant cooling occurs over central Asia and India. The SAI-induced strengthening of the wintertime stratospheric NH polar vortex can propagate down to the surface, resulting in a
340   pattern of sea-level pressure changes in the North Atlantic projecting onto a positive phase of the North Atlantic Oscillation (NAO), i.e., a significant reduction in sea level pressure over the Arctic region and a significant increase south of it (Figure 11, top-right) (Banerjee et al., 2021; Jones et al., 2021; Wunderlin et al., 2024). The described temperature responses in the NH in senD2-sai are a typical signal of the positive NAO. They are also associated with changes in precipitation consisting of drying over southern Europe and wettening over northern Europe (Figure 10, right panel) as storm tracks shift northward, as also
345   discussed in earlier studies (e.g., Haywood et al., 2022; Bednarz et al., 2023). The small but statistically significant cooling in the North Atlantic near Greenland is simulated in senD2-sai despite any changes in SSTs found in the coupled SSP2-4.5 SAI run. Therefore, we concluded for the interactive SSP2-4.5 SAI experiment, that besides changes in AMOC, some of the cooling in the North Atlantic has been induced by the stratosphere-troposphere coupling response to SAI, as SSP2-4.5 SAI also shows
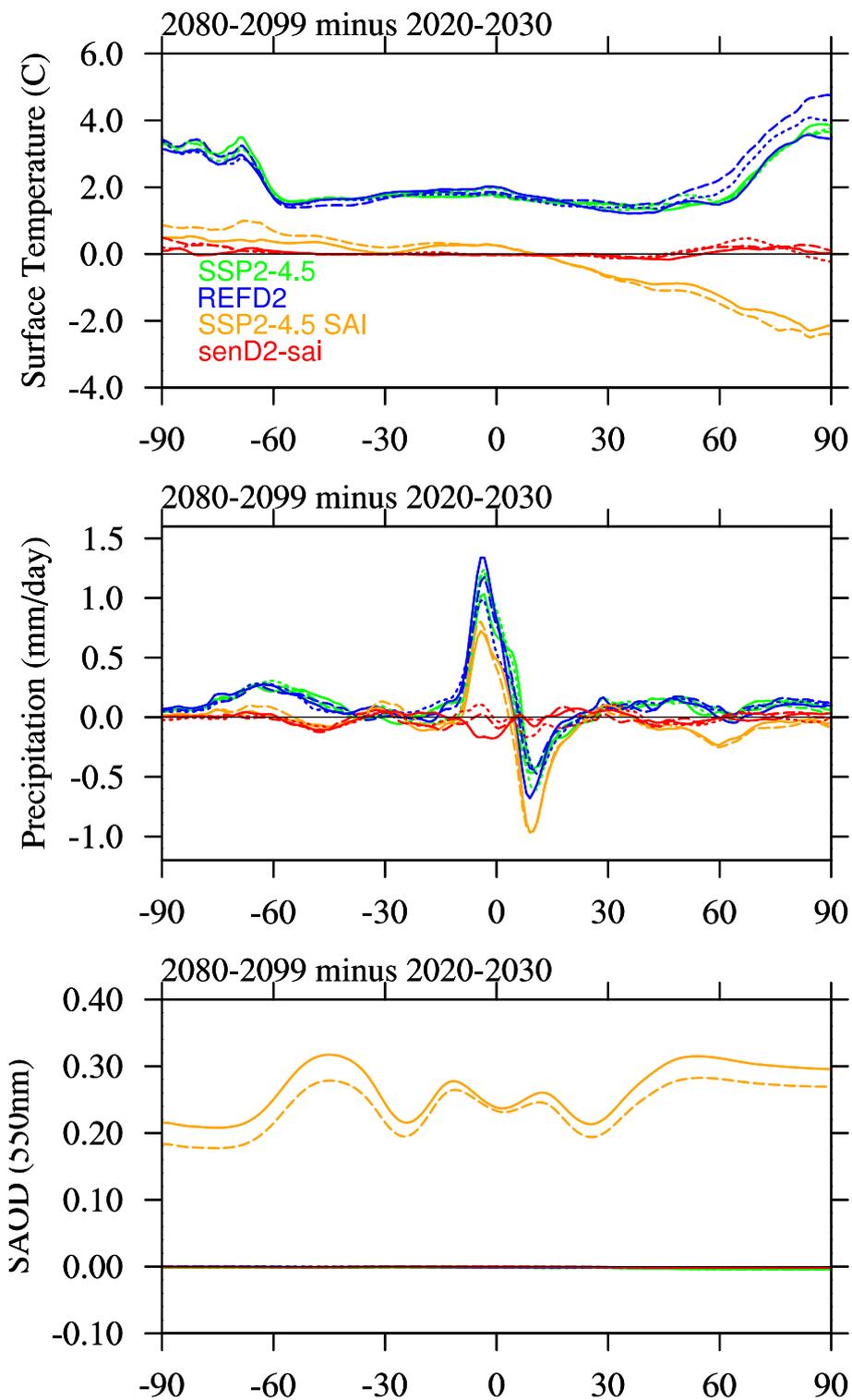
Figure 8. Zonal mean differences between 2080 – 2099 future experiments and 2020 – 2030 control experiments for the available ensemble members (see table 1), for near surface temperature (top), precipitation (middle), and Stratospheric Aerosol Optical Depth (SAOD) (bottom).
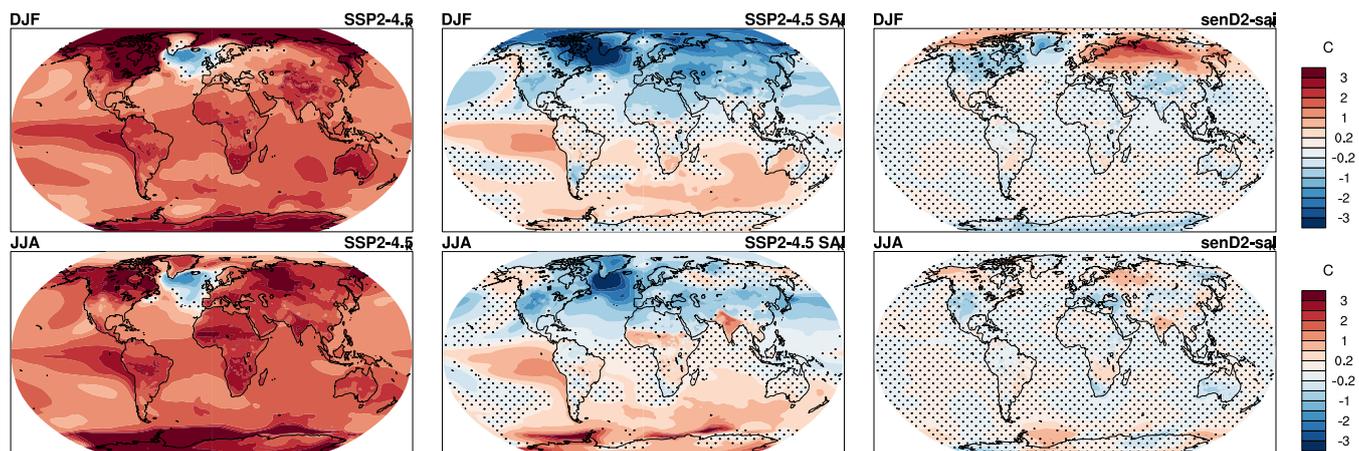
Figure 9. Ensemble-mean differences between 2080 – 2099 future experiments and 2020 – 2030 control experiments for near surface temperature in December/January/February (top) and June/July/August (bottom) for SSP2-4.5 (left), SSP2-4.5 SAI (middle) and senD2-sai (right). Areas of non-significant difference at the 95th % level to the control are marked as small black dots.
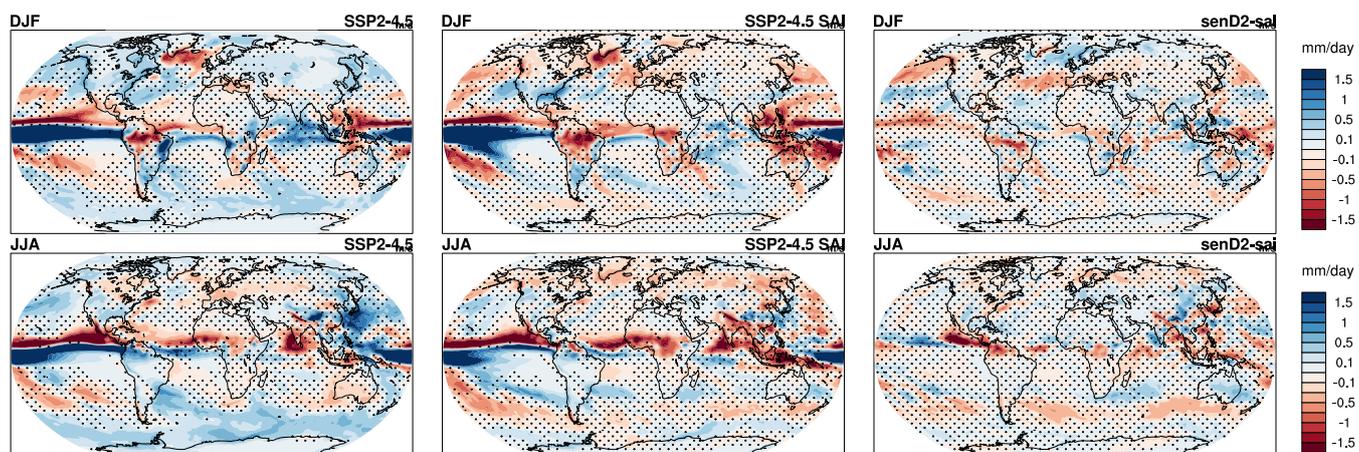
Figure 10. Ensemble-mean differences between 2080 – 2099 future experiments and 2020 –2030 control experiments for precipitation in December/January/February (top) and June/July/August (bottom) for SSP2-4.5 (left), SSP2-4.5 SAI (middle) and senD2-sai (right). Areas of non-significant difference at the 95th % level to the control are marked as small black dots.

the positive NAO sea-level pressure pattern (Figure 11). Furthermore, the sea-level pressure response in senD2-sai is zonally
350   symmetric in origin, with midlatitude sea-level pressure increasing not only in the Atlantic but also in the Pacific Aleutian
Low region. This is unlike the negative sea-level response, i.e., strengthening of the Aleutian Low, simulated in SSP2-4.5 SAI
discussed above, where teleconnections with the ocean variability dominated the response in the region.

Analogous to what happens in the NH, changes in the strength of the SH stratospheric polar vortex can also be coupled
with surface variability, and in this case, this modulation occurs via changes to the Southern Annual Mode (SAM). In both
355   SSP2-4.5 SAI and senD2-sai, the strengthening of the Antarctic polar vortex in austral winter (JJA) results in reduced sea
level pressure over the Antarctic continent and an increase in sea-level pressure over the Southern Ocean (Figure 12), a pattern
similar to the positive phase of SAM. This response is slightly more significant in senD2-sai than in SSP2.4-5 SAI and,
therefore, directly induced by the stratospheric top-down influence. The fixed SST experiment thus supports the suggestions
by Bednarz et al. (2022) that a response caused by SAI-induced stratospheric heating can result in a positive SAM. In austral
360   summer, however, while senD2-sai still shows a suggestion (albeit not strongly statistically significant) of a positive SAM-like
response, the coupled SSP2-4.5 SAI shows the opposite sign response, i.e., an increase in sea-level pressure over the Antarctic
and a decrease in mid-latitudes. This corresponds to the negative phase of SAM, and is accompanied by a significant weakening
of the SH tropospheric winds at 60S (Figure 5), not reproduced by the senD2-sai experiment. This austral summer negative
SAM and weakening of eddy-driven jet are therefore likely connected to the equatorial Pacific and the El-Nino-like response
365   resulting in changes in tropospheric winds and Kelvin wave fluxes into the stratosphere to contribute to the winter and spring
stratospheric easterly response. A similar relationship has also been found from observations and simple modeling studies
(L'Heureux and Thompson, 2006). However, an additional stratospheric-induced contribution from the springtime weakening
of the vortex can also not be ruled out as the result of the Antarctic ozone increases from reduced ODS and less SAD in
SSP2-4.5 compared to senD2-sai (see Section 3.1).

370   Differences in near-surface temperature in JJA in senD2-sai are, for the most part, insignificant, especially in the NH,
where the reductions in the subtropical jet are not reaching the surface and, therefore, not significantly affecting near-surface
temperatures (Figure 5, right bottom panel). Other small near-surface temperature changes in JJA in senD2-sai include cooling
over Southern Europe and the central US, as well as some cooling over South Australia and South Africa, and some warming
in Northern Europe and Alaska, parts of South Africa and East of the Antarctic Peninsula. These changes may be related to
375   additional land feedbacks that have to be further explored in multi-model comparison studies.

The SSP2-4.5 and refD2 simulations without SAI show a similar increase in global mean rainfall with increasing near-
surface temperatures (Figure 1, middle panel). On the other hand, SSP2-4.5 SAI and senD2-sai show a precipitation reduction
compared to the present day, which is significant about ten years after the start of SAI. This global mean rainfall reduction
is slightly stronger in the coupled SSP2-4.5 SAI compared to senD2-sai. Different processes are likely to contribute to this
380   difference, including the slightly stronger SAI-induced heating in the lower stratosphere, resulting in a greater enhancement
in tropospheric static stability (Ferraro et al., 2014; Lee et al., 2023) and additional feedback with the ocean resulting from the
uneven interhemispheric cooling and the El-Nino like response, which is only included in the coupled SSP2-4.5 SAI but not
in senD2-sai. Furthermore, zonally averaged changes in precipitation show a similar strengthening of tropical rainfall in the

SH and a weakening in the NH for both SSP2-4.5 and refD2 simulations without SAI (Figure 8, middle panel). The response
385   indicates a southward shift of the Intertropical Convergence Zone (ITCZ) under rising GHG levels (Figure S3, Supplement).
The coupled SSP2-4.5 SAI simulations also show a similar tropical precipitation shift compared to the control, with a relative
reduction on both sides of the equator, therefore amplifying the negative values in the NH and reducing the positive values in
the SH compared to SSP2-4.5 without SAI compared to the control in 2020 – 2030. Therefore, symmetric SAI in WACCM6
counters some of the increase in precipitation in the SH tropics but further reduces precipitation in the NH (Figure 8, middle
390   panel). Consistently, SSP2-4.5 SAI simulations project a reduced rainfall increase in JJA in the western Pacific, aligned with the
El Nino signal with SAI compared to the control. Such a response is aligned with a weakening of the Hadley Circulation under
SAI, as identified for similar experiments in (Bednarz et al., 2023). Furthermore, Bednarz et al. (2023) found an eastward shift
of the Walker circulation with SAI for 30°N, 30°S injections associated with surface temperature changes in the equatorial
Pacific and the resulting reductions in rainfall over the Maritime Continent and Australia, as can also be seen in SSP2-4.5 SAI
395   (Figure 10).

In general, precipitation changes in senD2-sai are, for the most part, not significant at the 95th % level of the t-test. The
minimized changes in near-surface air temperatures in senD2-sai compared to SSP2-4.5 SAI, in particular the significant
hemispheric asymmetry that was otherwise seen in the coupled ocean SSP2-4.5 SAI run, prevent shifts in the Hadley (and
Walker) Circulation, and thus the associated large-scale shifts in precipitation. The exceptions are the drying over South-West
400   Europe, a wettening of Northern Europe in DJF, and a wettening of Western Europe and drying of Northern Europe in JJA due
to the changes in the NAO sea-level pressure patterns (discussed above). Other signatures include increased precipitation over
Australia and the ocean at similar latitudes, while a drying occurs in the Southern Ocean. This zonal pattern is a signature of
the concurrent poleward shift in the tropospheric eddy-driven jet (Figure 5) and a positive SAM-like response (Figure 12) in
JJA. Significant reductions in rainfall also occur over central Africa, Venezuela, and Colombia, regions with strong tropical
405   convection that are likely impacted by increased static stability with SAI (Ferraro et al., 2014). Since senD2-sai included fixed
SSTs, precipitation changes cannot be a result of any El Nino-like response and its teleconnections and, therefore, are either
driven by the top-down dynamical changes and/or induced in part by changes in evaporation induced by the land feedback to
SAI.

4   Conclusions

410   The proposed CCMI-2022 senD2-sai experiment has been designed for multi-model comparison studies to investigate the ef-
fects of SAI on stratospheric chemistry and dynamics. The constrained experimental setup using a prescribed stratospheric
aerosol distribution and fixed SSTs and sea ice successfully isolates the SAI-induced stratosphere-controlled (top-down) pro-
cesses from ocean processes and their feedbacks with the atmosphere. This allows inter-model responses and their differences
to be identified while employing the same prescribed stratospheric aerosol perturbation. These differences can be attributed to
415   the resulting impacts on stratospheric chemistry, radiation, and dynamics rather than the (underlying) aerosol forcing. This pa-
per provides a detailed description of the CCMI-2022 SAI experiment. It further outlines the WACCM6 experiment to produce
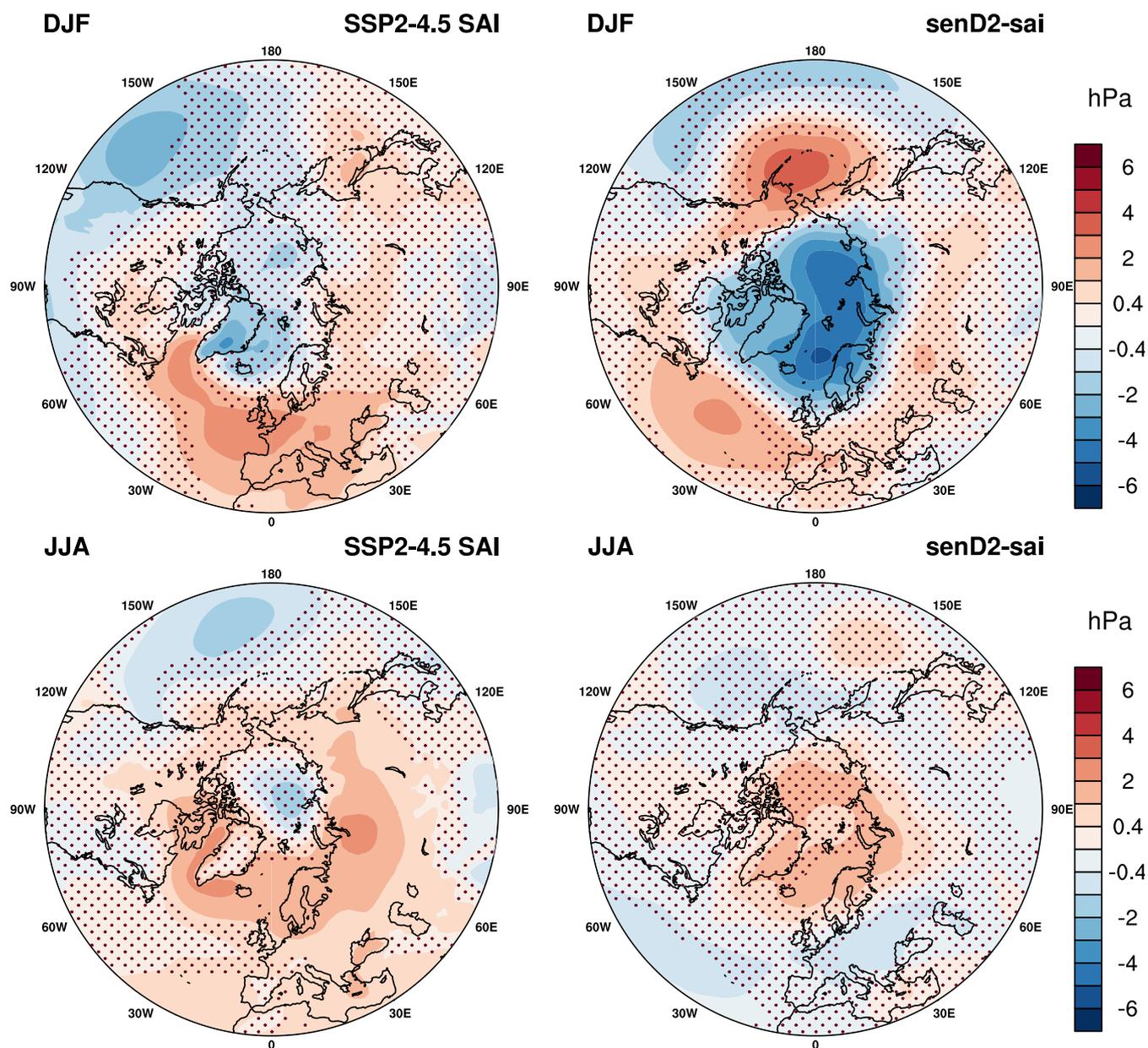
Figure 11. North polar view of ensemble-mean differences between 2080 – 2099 future experiments and 2020 – 2030 control experiments for sea level pressure in December/January/February (top) and June/July/August (bottom) for SSP2-4.5 (left), SSP2-4.5 SAI (middle) and senD2-sai (right). Areas of non-significant difference at the 95th % level to the control are marked as small black dots.
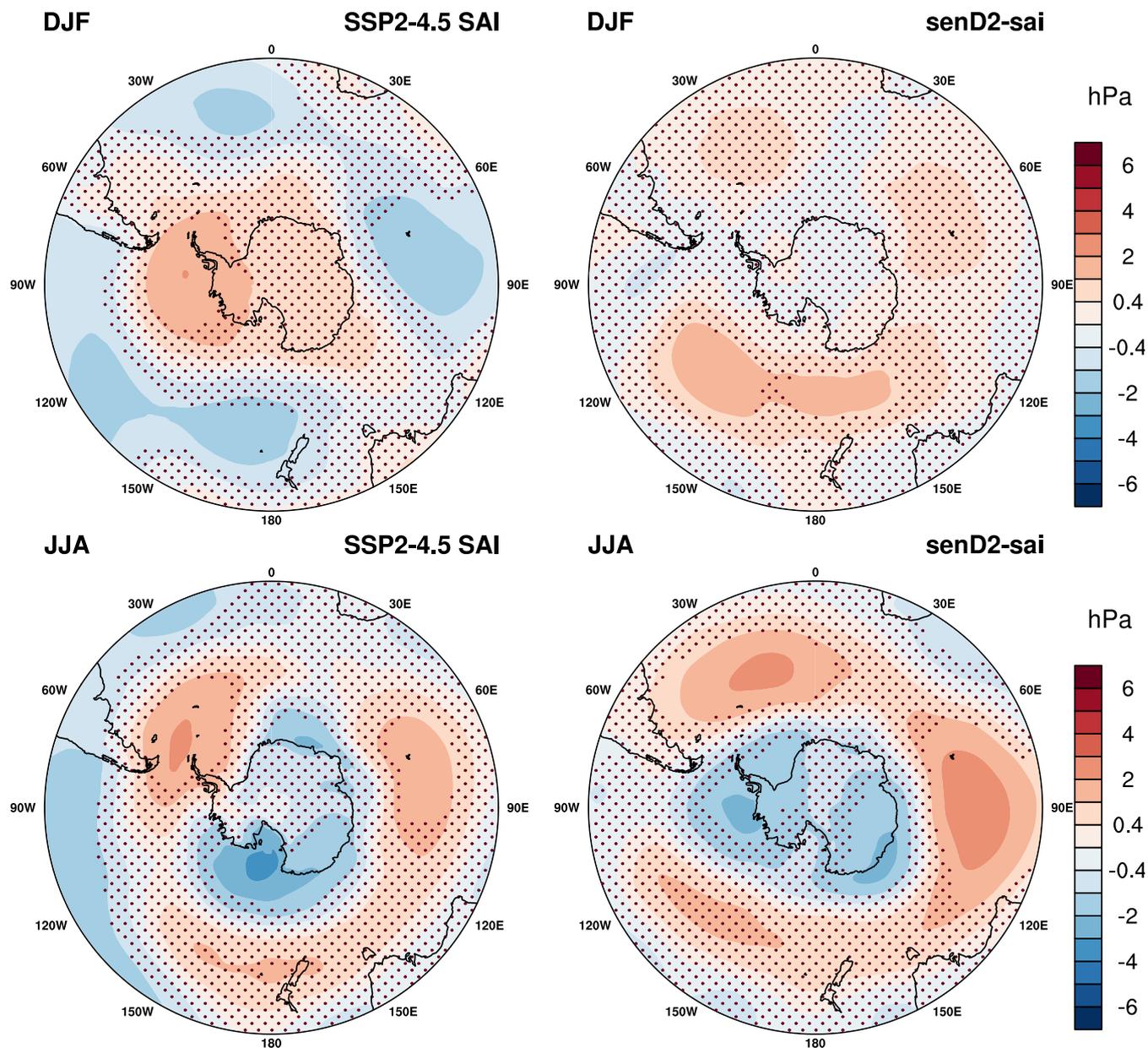
Figure 12. South polar view of ensemble-mean differences between 2080 – 2099 future experiments and 2020 – 2030 control experiments for sea level pressure in December/January/February (top) and June/July/August (bottom) for SSP2-4.5 (left), SSP2-4.5 SAI (middle) and senD2-sai (right). Areas of non-significant difference at the 95th % level to the control are marked as small black dots.

the recommended aerosol distribution and compares the results to the corresponding CCMI-2022 senD2-sai experiment. In addition, we summarize the tool that produces model-specific input variables from the provided stratospheric aerosol distribution. We also compare SAI-induced responses in stratospheric dynamics and chemistry (ozone and water vapor) along with surface

420   climate variables between a fully interactive experiment SSP2-4.5 SAI and the constrained CCMI-2022 senD2-sai experiment using WACCM6.

The setup of the WACCM6 interactive simulation to produce the stratospheric aerosol distribution for the CCMI-2022 senD2-sai experiment used symmetric (equal) injections in each hemisphere. This setup resulted in hemispherically close to symmetric aerosol and AOD distribution desired for multi-model comparisons of SAI stratospheric chemistry and dynamics

425   impacts. However, this setup in WACCM6 results in hemispherically unsymmetrical near-surface temperature cooling due to model-specific internal adjustments, including cloud and climate feedbacks. In addition, results show significant equatorial warming in the eastern Pacific related to a positive phase of the El Nino Southern Oscillation and its associated global-scale teleconnections. While undoubtedly important, these ocean climate feedbacks, including changes in AMOC, remain relatively uncertain and often poorly represented in the current climate models, which is a likely reason for significant uncertainties in

430   the regional climate response with SAI, especially in the tropics. Using a prescribed stratospheric aerosol distribution with climatological model-specific SSTs and sea ice for 2020 – 2030 conditions removes these uncertainties in the SAI-induced climate response in models. The setup also removes the potential for an over or under-cooling of models using a prescribed aerosol distribution from a different model (Zhang et al., 2024a).

The senD2-sai CCMI experiment is designed to understand inter-model differences in the stratosphere, assuming that the

435   differences between the fully interactive simulation and a simplified senD2-sai simulation are relatively small, as shown here. Some differences are still expected due to small differences in the details of aerosol properties and distributions from the coupled run in a prescribed aerosol setup. In addition, the influences from the associated changes in ocean surface temperatures and sea ice can impact the wave activity entering the stratosphere and, therefore, change the responses to the BDC with SAI. Therefore, quantitative statements have to be considered with a caveat since results, e.g., changes in total column ozone, do

440   not reflect the full complexity of interactions. Here, we find that following the SSP2-4.5 GHG future scenario, the difference in SAI-induced changes in TCO between the interactive and the constrained experiment is only significant after 2060-2070, when SAI injections are relatively large (above 15 $TgSO_2$/yr) to counter more than 1°C of near-surface temperature increase. Some of the differences in this study may have also been introduced by using different ODS levels in SSP2-4.5 and SSP2-4.5 SAI compared to refD2 and senD2-sai.

445   Here, in addition to assessing processes in the stratosphere, we take advantage of this specific setup and can qualitatively investigate whether specific surface climate changes are driven by adjustments in the stratosphere or rather are based on the much slower response and feedbacks from the ocean, or both. We support findings from earlier studies, demonstrating that regional SAI-induced surface climate changes connected to the modulations of extra-tropical modes of variability (NAO in the NH, SAM in the SH) are driven by the top-down influence of stratospheric circulation responses as the result of aerosol-induced

450   stratospheric heating. In contrast to the extra-tropical changes, any surface climate responses in the tropics in senD2-sai are found to be very small and/or not statistically significant. Given the uncertainty in the model representation of ocean processes

and feedbacks, the constrained CCMI SAI experiment allows us to isolate the downward influence of SAI via changes in stratospheric dynamics across models while removing contribution from the ocean to the stratospheric variability. The in-depth assessment of SAI-induced changes in stratospheric chemistry and aerosols in a multi-model setup is an important mandate by
455 CCMI in support of the upcoming WMO assessment. We therefore encourage modeling group to take part in this important effort.

Code and data availability. All data used in this work is available from the Earth System Grid (https://esgf-node.llnl.gov/search/cmip6/)

Author contributions. ST performed model simulations, analyzed the analyses of results, and outlined and wrote the manuscript. EMB analyzed the results and helped outline and write the manuscript. DK performed some of the simulations used in this paper and contributed
460 to writing the manuscript. AJ, DV, GC, DP contributed in writing the manuscript and in the outline of the paper.

Competing interests. The authors declare no competing interests. ST and EMB are members of the editorial board of the journal.

Acknowledgements. The CESM project is supported primarily by the National Science Foundation. This material is based upon work supported by the National Center for Atmospheric Research, which is a major facility sponsored by the NSF under Cooperative Agreement No. 1852977. Computing and data storage resources, including the Cheyenne supercomputer (doi:10.5065/D6RX99HX), were provided by the
465 Computational and Information Systems Laboratory (CISL) at NCAR. Support for EMB has been provided by the National Oceanic and Atmospheric Administration (NOAA) cooperative agreement (NA22OAR4320151) and the Earth's Radiative Budget (ERB) program. G.C. acknowledges funding from the European Commission via the ERC StG 101078127.

References

Abalos, M., Calvo, N., Benito-Barca, S., Garny, H., Hardiman, S. C., Lin, P., Andrews, M. B., Butchart, N., Garcia, R., Orbe, C., Saint-Martin,
470   D., Watanabe, S., and Yoshida, K.: The Brewer–Dobson circulation in CMIP6, Atmospheric Chemistry and Physics, 21, 13 571–13 591,
        https://doi.org/10.5194/acp-21-13571-2021, https://acp.copernicus.org/articles/21/13571/2021/, 2021.

Banerjee, A., Butler, A. H., Polvani, L. M., Robock, A., Simpson, I. R., and Sun, L.: Robust winter warming over Eurasia un-
        der stratospheric sulfate geoengineering – the role of stratospheric dynamics, Atmospheric Chemistry and Physics, 21, 6985–6997,
        https://doi.org/10.5194/acp-21-6985-2021, https://acp.copernicus.org/articles/21/6985/2021/, 2021.

475   Bednarz, E. M., Visioni, D., Banerjee, A., Braesicke, P., Kravitz, B., and MacMartin, D. G.: The Overlooked Role of
        the Stratosphere Under a Solar Constant Reduction, Geophysical Research Letters, 49, https://doi.org/10.1029/2022GL098773,
        https://agupubs.onlinelibrary.wiley.com/doi/10.1029/2022GL098773, 2022.

Bednarz, E. M., Butler, A. H., Visioni, D., Zhang, Y., Kravitz, B., and MacMartin, D. G.: Injec-
        tion strategy – a driver of atmospheric circulation and ozone response to stratospheric aerosol geoengi-
480   neering, Atmospheric Chemistry and Physics, 23, 13 665–13 684, https://doi.org/10.5194/acp-23-13665-2023,
        https://egusphere.copernicus.org/preprints/2023/egusphere-2023-495/https://acp.copernicus.org/articles/23/13665/2023/, 2023.

Bohren, C. F. and Huffman, D. R.: Absorption and Scattering of Light by Small Particles, Wiley, https://doi.org/10.1002/9783527618156,
        https://onlinelibrary.wiley.com/doi/book/10.1002/9783527618156, 1998.

Butchart, N., Cionni, I., Eyring, V., Shepherd, T. G., Waugh, D. W., Akiyoshi, H., Austin, J., Brühl, C., Chipperfield, M. P., Cordero, E.,
485   Dameris, M., Deckert, R., Dhomse, S., Frith, S. M., Garcia, R. R., Gettelman, A., Giorgetta, M. A., Kinnison, D. E., Li, F., Mancini,
        E., McLandress, C., Pawson, S., Pitari, G., Plummer, D. A., Rozanov, E., Sassi, F., Scinocca, J. F., Shibata, K., Steil, B., and Tian, W.:
        Chemistry–Climate Model Simulations of Twenty-First Century Stratospheric Climate and Circulation Changes, Journal of Climate, 23,
        5349–5374, https://doi.org/10.1175/2010JCLI3404.1, http://journals.ametsoc.org/doi/10.1175/2010JCLI3404.1, 2010.

Danabasoglu, G., Lamarque, J.-F., Bachmeister, J., Bailey, D. A., DuVivier, A. K., and et al. Edwards, J.: The Commu-
490   nity Earth System Model version 2 (CESM2), Journal of Advances in Modeling Earth Systems, 12, e2019MS001 916,
        https://agupubs.onlinelibrary.wiley.com/doi/full/10.1029/2019MS001916, 2020.

Domeisen, D. I., Garfinkel, C. I., and Butler, A. H.: The Teleconnection of El Niño Southern Oscillation to the Stratosphere, Reviews
        of Geophysics, 57, 5–47, https://doi.org/10.1029/2018RG000596, https://agupubs.onlinelibrary.wiley.com/doi/10.1029/2018RG000596,
        2019.

495   Emmons, L. K., Schwantes, R. H., Orlando, J. J., Tyndall, G., Kinnison, D., Lamarque, J., Marsh, D., Mills, M. J., Tilmes, S., Bardeen,
        C., Buchholz, R. R., Conley, A., Gettelman, A., Garcia, R., Simpson, I., Blake, D. R., Meinardi, S., and Pétron, G.: The Chem-
        istry Mechanism in the Community Earth System Model Version 2 (CESM2), Journal of Advances in Modeling Earth Systems, 12,
        https://doi.org/10.1029/2019MS001882, https://agupubs.onlinelibrary.wiley.com/doi/10.1029/2019MS001882, 2020.

Eyring, V., Shepherd, T. G., and Waugh, D. W., eds.: SPARC Report on the Evaluation of Chemistry-Climate Models, {SPARC} Report No.
500   5, WCRP-132, WMO/TD-No.1526, 2010.

Fasullo, J. T. and Richter, J. H.: Dependence of strategic solar climate intervention on background scenario and model physics, Atmospheric
        Chemistry and Physics, 23, 163–182, https://doi.org/10.5194/acp-23-163-2023, https://acp.copernicus.org/articles/23/163/2023/, 2023.

Ferraro, A. J., Highwood, E. J., and Charlton-Perez, A. J.: Weakened tropical circulation and reduced precipitation in re-
sponse to geoengineering, Environmental Research Letters, 9, 014 001, https://doi.org/10.1088/1748-9326/9/1/014001,
505   http://stacks.iop.org/1748-9326/9/i=1/a=014001?key=crossref.878d5812d41285f5514acaa5402e63c3, 2014.

Frith, S. M., Stolarski, R. S., Kramarova, N. A., and McPeters, R. D.: Estimating uncertainties in the SBUV Version 8.6
merged profile ozone data set, Atmospheric Chemistry and Physics, 17, 14 695–14 707, https://doi.org/10.5194/acp-17-14695-2017,
https://acp.copernicus.org/articles/17/14695/2017/, 2017.

Gettelman, A., Mills, M. J., Kinnison, D. E., Garcia, R. R., Smith, A. K., Marsh, D. R., Tilmes, S., Vitt, F., Bardeen, C. G., McIner-
510   ney, J., Liu, H.-L., Solomon, S. C., Polvani, L. M., Emmons, L. K., Lamarque, J.-F., Richter, J. H., Glanville, A. S., Bacmeister, J. T.,
Phillips, A. S., Neale, R. B., Simpson, I. R., DuVivier, A. K., Hodzic, A., and Randel, W. J.: The Whole Atmosphere Community Climate
Model Version 6 (WACCM6), Journal of Geophysical Research: Atmospheres, p. 2019JD030943, https://doi.org/10.1029/2019JD030943,
https://onlinelibrary.wiley.com/doi/abs/10.1029/2019JD030943, 2019.

Haigh, J. D. and Pyle, J. A.: Ozone perturbation experiments in a two-dimensional circulation model, Quar-
515   terly Journal of the Royal Meteorological Society, 108, 551–574, https://doi.org/10.1002/qj.49710845705,
https://rmets.onlinelibrary.wiley.com/doi/10.1002/qj.49710845705, 1982.

Hardiman, S. C., Butchart, N., and Calvo, N.: The morphology of the Brewer-Dobson circulation and its response to climate change
in CMIP5 simulations, Quarterly Journal of the Royal Meteorological Society, 140, 1958–1965, https://doi.org/10.1002/qj.2258,
https://onlinelibrary.wiley.com/doi/10.1002/qj.2258, 2014.

520   Haywood, J. M., Jones, A., Johnson, B. T., and McFarlane Smith, W.: Assessing the consequences of including aerosol absorp-
tion in potential stratospheric aerosol injection climate intervention strategies, Atmospheric Chemistry and Physics, 22, 6135–6150,
https://doi.org/10.5194/acp-22-6135-2022, https://acp.copernicus.org/articles/22/6135/2022/, 2022.

Henry, M., Haywood, J., Jones, A., Dalvi, M., Wells, A., Visioni, D., Bednarz, E. M., MacMartin, D. G., Lee, W., and Tye, M. R.: Comparison
of UKESM1 and CESM2 simulations using the same multi-target stratospheric aerosol injection strategy, Atmospheric Chemistry and
525   Physics, 23, 13 369–13 385, https://doi.org/10.5194/acp-23-13369-2023, https://acp.copernicus.org/articles/23/13369/2023/, 2023.

Jones, A., Haywood, J. M., Jones, A. C., Tilmes, S., Kravitz, B., and Robock, A.: North Atlantic Oscillation response
in GeoMIP experiments G6solar and G6sulfur: why detailed modelling is needed for understanding regional implications
of solar radiation management, Atmospheric Chemistry and Physics, 21, 1287–1304, https://doi.org/10.5194/acp-21-1287-2021,
https://acp.copernicus.org/articles/21/1287/2021/, 2021.

530   Jörimann, A., Sukhodolov, T., Luo, B., Chiodo, G., Mann, G. W., and Peter, T.: A REtrieval Method for optical and physical Aerosol
Properties in the stratosphere (REMAPv1), Geoscientific Model Development Discussions, p. to be submitted, 2024.

Karpechko, A. Y., Afargan-Gerstman, H., Butler, A. H., Domeisen, D. I. V., Kretschmer, M., Lawrence, Z., Manzini, E., Sigmond,
M., Simpson, I. R., and Wu, Z.: Northern Hemisphere Stratosphere-Troposphere Circulation Change in CMIP6 Models: 1. Inter-
Model Spread and Scenario Sensitivity, Journal of Geophysical Research: Atmospheres, 127, https://doi.org/10.1029/2022JD036992,
535   https://agupubs.onlinelibrary.wiley.com/doi/10.1029/2022JD036992, 2022.

Keeble, J., Hassler, B., Banerjee, A., Checa-Garcia, R., Chiodo, G., Davis, S., Eyring, V., Griffiths, P. T., Morgenstern, O., Nowack, P.,
Zeng, G., Zhang, J., Bodeker, G., Burrows, S., Cameron-Smith, P., Cugnet, D., Danek, C., Deushi, M., Horowitz, L. W., Kubin, A., Li,
L., Lohmann, G., Michou, M., Mills, M. J., Nabat, P., Olivié, D., Park, S., Seland, Ø., Stoll, J., Wieners, K.-H., and Wu, T.: Evaluating
stratospheric ozone and water vapour changes in CMIP6 models from 1850 to 2100, Atmospheric Chemistry and Physics, 21, 5015–5061,
540   https://doi.org/10.5194/acp-21-5015-2021, https://acp.copernicus.org/articles/21/5015/2021/, 2021.

Kinnison, D. E., Brasseur, G. P., Walters, S., Garcia, R. R., Marsch, D. A., Sassi, F., Boville, B. A., Harvey, V. L., Randall, C. E., Emmons, L., Lamarque, J. F., Hess, P., Orlando, J. J., Tie, X. X., Randel, W., Pan, L. L., Gettelman, A., Granier, C., Diehl, T., Niemaier, U., and Simmons, A. J.: Sensitivity of chemical tracers to meteorological parameters in the MOZART-3 chemical transport model, J.Geophys. Res., 112, D20 302, https://doi.org/10.1029/2006JD007879, 2007.

545 Kravitz, B., MacMartin, D. G., Mills, M. J., Richter, J. H., Tilmes, S., Lamarque, J.-F., Tribbia, J. J., and Vitt, F.: First Simulations of Designing Stratospheric Sulfate Aerosol Geoengineering to Meet Multiple Simultaneous Climate Objectives, Journal of Geophysical Research: Atmospheres, 122, https://doi.org/10.1002/2017JD026874, 2017.

Lawrence, D. M., Fisher, R. A., Koven, C. D., Oleson, K. W., Swenson, S. C., Bonan, G., Collier, N., Ghimire, B., Kampenhout, L., Kennedy, D., Kluzek, E., Lawrence, P. J., Li, F., Li, H., Lombardozzi, D., Riley, W. J., Sacks, W. J., Shi, M., Vertenstein, M., Wieder,
550 W. R., Xu, C., Ali, A. A., Badger, A. M., Bisht, G., Broeke, M., Brunke, M. A., Burns, S. P., Buzan, J., Clark, M., Craig, A., Dahlin, K., Drewniak, B., Fisher, J. B., Flanner, M., Fox, A. M., Gentine, P., Hoffman, F., Keppel-Aleks, G., Knox, R., Kumar, S., Lenaerts, J., Leung, L. R., Lipscomb, W. H., Lu, Y., Pandey, A., Pelletier, J. D., Perket, J., Randerson, J. T., Ricciuto, D. M., Sanderson, B. M., Slater, A., Subin, Z. M., Tang, J., Thomas, R. Q., Val Martin, M., and Zeng, X.: The Community Land Model version 5: Description of new features, benchmarking, and impact of forcing uncertainty, Journal of Advances in Modeling Earth Systems, p. 2018MS001583,
555 https://doi.org/10.1029/2018MS001583, https://onlinelibrary.wiley.com/doi/abs/10.1029/2018MS001583, 2019.

Lee, W. R., Visioni, D., Bednarz, E. M., MacMartin, D. G., Kravitz, B., and Tilmes, S.: Quantifying the Efficiency of Stratospheric Aerosol Geoengineering at Different Altitudes, Geophysical Research Letters, 50, https://doi.org/10.1029/2023GL104417, https://agupubs.onlinelibrary.wiley.com/doi/10.1029/2023GL104417, 2023.

L'Heureux, M. L. and Thompson, D. W. J.: Observed Relationships between the El Niño–Southern Oscillation and
560 the Extratropical Zonal-Mean Circulation, Journal of Climate, 19, 276–287, https://doi.org/10.1175/JCLI3617.1, http://journals.ametsoc.org/doi/10.1175/JCLI3617.1, 2006.

Li, H., Richter, J. H., Hu, A., Meehl, G. A., and MacMartin, D.: Responses in the Subpolar North Atlantic in Two Climate Model Sensitivity Experiments with Increased Stratospheric Aerosols, Journal of Climate, 36, 7675–7688, https://doi.org/10.1175/JCLI-D-23-0225.1, https://journals.ametsoc.org/view/journals/clim/36/21/JCLI-D-23-0225.1.xml, 2023.

565 Liu, X., Ma, P. L., Wang, H., Tilmes, S., Singh, B., Easter, R. C., Ghan, S. J., and Rasch, P. J.: Description and evaluation of a new four-mode version of the Modal Aerosol Module (MAM4) within version 5.3 of the Community Atmosphere Model, Geoscientific Model Development, 9, 505–522, https://doi.org/10.5194/gmd-9-505-2016, 2016.

MacMartin, D. G., Kravitz, B., Tilmes, S., Richter, J. H., Mills, M. J., Lamarque, J.-F., Tribbia, J. J., and Vitt, F.: The Climate Response to Stratospheric Aerosol Geoengineering Can Be Tailored Using Multiple Injection Locations, Journal of Geophysical Research: Atmo-
570 spheres, 122, https://doi.org/10.1002/2017JD026868, 2017.

Malik, A., Nowack, P. J., Haigh, J. D., Cao, L., Atique, L., and Plancherel, Y.: Tropical Pacific climate variability under solar geoengineering: impacts on ENSO extremes, Atmospheric Chemistry and Physics, 20, 15 461–15 485, https://doi.org/10.5194/acp-20-15461-2020, https://acp.copernicus.org/articles/20/15461/2020/, 2020.

McLandress, C., Jonsson, A. I., Plummer, D. A., Reader, M. C., Scinocca, J. F., and Shepherd, T. G.: Separating the Dynamical
575 Effects of Climate Change and Ozone Depletion. Part I: Southern Hemisphere Stratosphere, Journal of Climate, 23, 5002–5020, https://doi.org/10.1175/2010JCLI3586.1, http://journals.ametsoc.org/doi/10.1175/2010JCLI3586.1, 2010.

Meinshausen, M., Vogel, E., Nauels, A., Lorbacher, K., Meinshausen, N., Etheridge, D. M., Fraser, P. J., Montzka, S. A., Rayner, P. J., Trudinger, C. M., Krummel, P. B., Beyerle, U., Canadell, J. G., Daniel, J. S., Enting, I. G., Law, R. M., Lunder, C. R., O'Doherty, S.,

Prinn, R. G., Reimann, S., Rubino, M., Velders, G. J. M., Vollmer, M. K., Wang, R. H. J., and Weiss, R.: Historical greenhouse gas concentrations for climate modelling (CMIP6), Geoscientific Model Development, 10, 2057–2116, https://doi.org/10.5194/gmd-10-2057-2017, https://www.geosci-model-dev.net/10/2057/2017/, 2017.

Mills, M. J., Richter, J. H., Tilmes, S., Kravitz, B., MacMartin, D. G., Glanville, A. A., Tribbia, J. J., Lamarque, J.-F., Vitt, F., Schmidt, A., Gettelman, A., Hannay, C., Bacmeister, J. T., and Kinnison, D. E.: Radiative and chemical response to interactive stratospheric sulfate aerosols in fully coupled CESM1(WACCM), Journal of Geophysical Research: Atmospheres, 122, https://doi.org/10.1002/2017JD027006, 2017.

Niemeier, U., Richter, J. H., and Tilmes, S.: Differing responses of the quasi-biennial oscillation to artificial SO2 injections in two global models, Atmospheric Chemistry and Physics, 20, 8975–8987, https://doi.org/10.5194/acp-20-8975-2020, https://acp.copernicus.org/articles/20/8975/2020/, 2020.

Pitari, G., Aquila, V., Kravitz, B., Robock, A., Watanabe, S., Cionni, I., Luca, N. D., Genova, G. D., Mancini, E., and Tilmes, S.: Stratospheric ozone response to sulfate geoengineering: Results from the Geoengineering Model Intercomparison Project (GeoMIP), Journal of Geophysical Research: Atmospheres, 119, 2629–2653, https://doi.org/10.1002/2013JD020566, http://doi.wiley.com/10.1002/2013JD020566, 2014.

Plummer, D. and Co-authors: SPARC Scientific Steering Group Newsletter, pp. 22–30, 2021.

Rezaei, A., Karami, K., Tilmes, S., and Moore, J. C.: Changes in global teleconnection patterns under global warming and stratospheric aerosol intervention scenarios, https://doi.org/10.5194/egusphere-2022-974, https://egusphere.copernicus.org/preprints/2022/egusphere-2022-974/, 2022.

Richter, J. H., Tilmes, S., Mills, M. J., Tribbia, J. J., Kravitz, B., MacMartin, D. G., Vitt, F., and Lamarque, J. F.: Stratospheric Dynamical Response to SO2 Injections, Journal of Geophysical Research Atmospheres, 122, 2017.

Richter, J. H., Visioni, D., MacMartin, D. G., Bailey, D. A., Rosenbloom, N., Dobbins, B., Lee, W. R., Tye, M., and Lamarque, J.-F.: Assessing Responses and Impacts of Solar climate intervention on the Earth system with stratospheric aerosol injection (ARISE-SAI): protocol and initial results from the first simulations, Geoscientific Model Development, 15, 8221–8243, https://doi.org/10.5194/gmd-15-8221-2022, https://gmd.copernicus.org/articles/15/8221/2022/, 2022.

Simpson, I. S., S.Tilmes, Richter, J. H., Kravitz, B., MacMartin, D. G., Mills, M. J., Fasullo, J. T., and Pendergrass, A. G.: The regional hydroclimate response to stratospheric sulfate geoengineering and the role of stratospheric heating, J.Geophys. Res. Geophysical Res., 2019.

Solomon, S., Kinnison, D., Bandoro, J., and Garcia, R.: Journal of Geophysical Research : Atmospheres Simulation of polar ozone depletion : An update, Journal of Geophysical Research D: Atmospheres, pp. 7958–7974, https://doi.org/10.1002/2015JD023365.Received, 2015.

Thomason, L. W., Ernest, N., Millán, L., Rieger, L., Bourassa, A., Vernier, J.-P., Manney, G., Luo, B., Arfeuille, F., and Peter, T.: A global space-based stratospheric aerosol climatology: 1979–2016, Earth System Science Data, 10, 469–492, https://doi.org/10.5194/essd-10-469-2018, https://essd.copernicus.org/articles/10/469/2018/, 2018.

Tilmes, S., Richter, J. H., Kravitz, B., MacMartin, D. G., Mills, M. J., Simpson, I. R., Glanville, A. S., Fasullo, J. T., Phillips, A. S., Lamarque, J.-F., Tribbia, J., Edwards, J., Mickelson, S., and Ghosh, S.: CESM1(WACCM) Stratospheric Aerosol Geoengineering Large Ensemble Project, Bulletin of the American Meteorological Society, 99, 2361–2371, https://doi.org/10.1175/BAMS-D-17-0267.1, http://journals.ametsoc.org/doi/10.1175/BAMS-D-17-0267.1, 2018a.

Tilmes, S., Richter, J. H., Mills, M. J., Kravitz, B., MacMartin, D. G., Garcia, R. R., Kinnison, D. E., Lamarque, J., Tribbia, J., and Vitt, F.: Effects of Different Stratospheric SO2 Injection Altitudes on Stratospheric Chemistry and Dynamics, Journal of Geophysical Research: Atmospheres, 123, 4654–4673, https://doi.org/10.1002/2017JD028146, https://onlinelibrary.wiley.com/doi/10.1002/2017JD028146, 2018b.

Tilmes, S., MacMartin, D. G., Lenaerts, J. T. M., van Kampenhout, L., Muntjewerf, L., Xia, L., Harrison, C. S., Krumhardt, K. M., Mills, M. J., Kravitz, B., and Robock, A.: Reaching 1.5 and 2.0C global surface temperature targets using stratospheric aerosol geoengineering, Earth System Dynamics, 11, 579–601, https://doi.org/10.5194/esd-11-579-2020, https://esd.copernicus.org/articles/11/579/2020/, 2020.

620 Tilmes, S., Visioni, D., Jones, A., Haywood, J., Séférian, R., Nabat, P., Boucher, O., Bednarz, E. M., and Niemeier, U.: Stratospheric ozone response to sulfate aerosol and solar dimming climate interventions based on the G6 Geoengineering Model Intercomparison Project (GeoMIP) simulations, Atmospheric Chemistry and Physics, 22, 4557–4579, https://doi.org/10.5194/acp-22-4557-2022, https://acp.copernicus.org/articles/22/4557/2022/, 2022.

Trenberth, K. E.: ENSO in the Global Climate System, pp. 21–37, https://doi.org/10.1002/9781119548164.ch2, 625 https://agupubs.onlinelibrary.wiley.com/doi/10.1002/9781119548164.ch2, 2020.

Visioni, D., MacMartin, D. G., and Kravitz, B.: Is Turning Down the Sun a Good Proxy for Stratospheric Sulfate Geoengineering?, Journal of Geophysical Research: Atmospheres, 126, https://doi.org/10.1029/2020JD033952, https://agupubs.onlinelibrary.wiley.com/doi/10.1029/2020JD033952, 2021a.

Visioni, D., MacMartin, D. G., Kravitz, B., Boucher, O., Jones, A., Lurton, T., Martine, M., Mills, M. J., Nabat, P., Niemeier, U., Séférian, R., 630 and Tilmes, S.: Identifying the sources of uncertainty in climate model simulations of solar radiation modification with the G6sulfur and G6solar Geoengineering Model Intercomparison Project (GeoMIP) simulations, Atmospheric Chemistry and Physics, 21, 10 039–10 063, https://doi.org/10.5194/acp-21-10039-2021, https://acp.copernicus.org/articles/21/10039/2021/, 2021b.

Visioni, D., Kravitz, B., Robock, A., Tilmes, S., Haywood, J., Boucher, O., Lawrence, M., Irvine, P., Niemeier, U., Xia, L., Chiodo, G., Lennard, C., Watanabe, S., Moore, J. C., and Muri, H.: Opinion: The scientific and community-building roles of the Geoengi- 635 neering Model Intercomparison Project (GeoMIP) – past, present, and future, Atmospheric Chemistry and Physics, 23, 5149–5176, https://doi.org/10.5194/acp-23-5149-2023, https://acp.copernicus.org/articles/23/5149/2023/, 2023.

WMO: Scientific assessment of ozone depletion: 2006, Global Ozone Research and Monitoring Project-Report No.\ 50, Geneva, Switzerland, 2007.

WMO: Scientific Assessment of Ozone Depletion, www.unep.ch/ozone/AssessmentPanels/SAP/ScientificAssessment2010/00-SAP-2010-Assement-report.pdf 640 2010.

WMO: Scientific Assessment of Ozone Depletion: 2018, Global Ozone Research and Monitoring Project–Report No. 58, Geneva, Switzerland, 2018.

WMO: Scientific Assessment of Ozone Depletion 2022, Global Ozone Research and Monitoring Project-Report No. 278, Geneva, Switzerland, 2022.

645 Wunderlin, E., Chiodo, G., Sukhodolov, T., Vattioni, S., Visioni, D., and Tilmes, S.: Side Effects of Sulfur-Based Geoengi- neering Due To Absorptivity of Sulfate Aerosols, Geophysical Research Letters, 51, https://doi.org/10.1029/2023GL107285, https://agupubs.onlinelibrary.wiley.com/doi/10.1029/2023GL107285, 2024.

Zhang, S., Naik, V., Paynter, D., Tilmes, S., and John, J.: Assessing GFDL-ESM4.1 Climate Responses to CESM2-WACCM6 Stratospheric Aerosol Injection for a 2.0°C Warming Target, Geophysical Research Letters, 2024a.

650 Zhang, Y., MacMartin, D. G., Visioni, D., Bednarz, E. M., and Kravitz, B.: Hemispherically symmetric strategies for stratospheric aerosol in- jection, Earth System Dynamics, 15, 191–213, https://doi.org/10.5194/esd-15-191-2024, https://esd.copernicus.org/articles/15/191/2024/, 2024b.
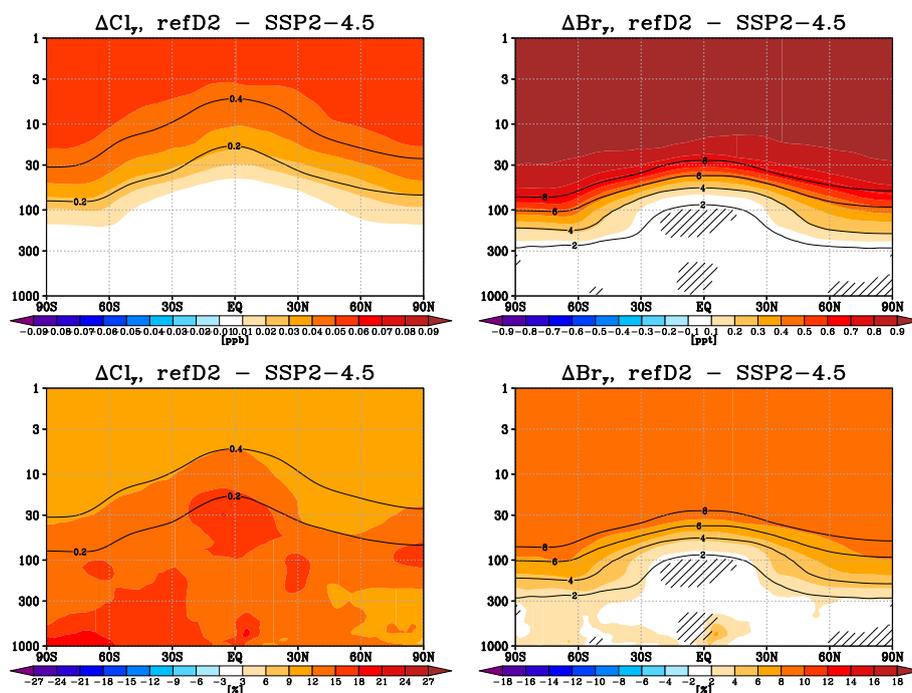
Figure A1. Zonal-mean absolute (top) and relative (bottom) changes in total Chlorine (Cl_y), left, and total bromine ((Br_y) (right) between refD2 and SSP2-4.5 scenarios for 2080–2099 conditions.

Table 1. Overview of modeling experiments

Experiment Name	GHG; ODS Scenario	Simulation Period	Ensemble Members	SSTs	Control Experiment 2020 – 2030
SSP2.4-5	SSP2.4-5	2015–2100	3	interactive	SSP2.4-5
refD2	SSP2.4-5; refD2 CFCs	2015–2100	3	interactive	refD2
SSP2.4-5 SAI	SSP2.4-5	2020 – 2100	2	interactive	SSP2.4-5
senD2-sai	SSP2.4-5; refD2 CFCs	2020 – 2100	3	prescribed (2020 – 2030)	senD2-fix
senD2-fix	SSP2.4-5; refD2 CFCs	2015 – 2035 (2100)	3	prescribed (2020 – 2030)	

Appendix A: Supporting Figures

This section includes supporting material in the form of additional Figures A1 to A3, as referred to in the main text.
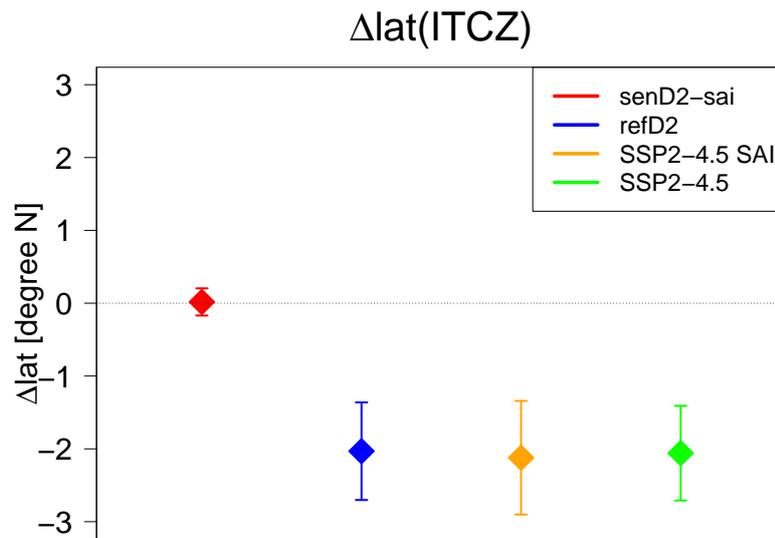
Figure A2. Differences of the annual mean and latitude of the Intertropical Convergence Zone (ITCZ) between 2080 – 2099 compared to 2010 – 2030 for different experiments (see legend), the standard error is shown as vertical bars.
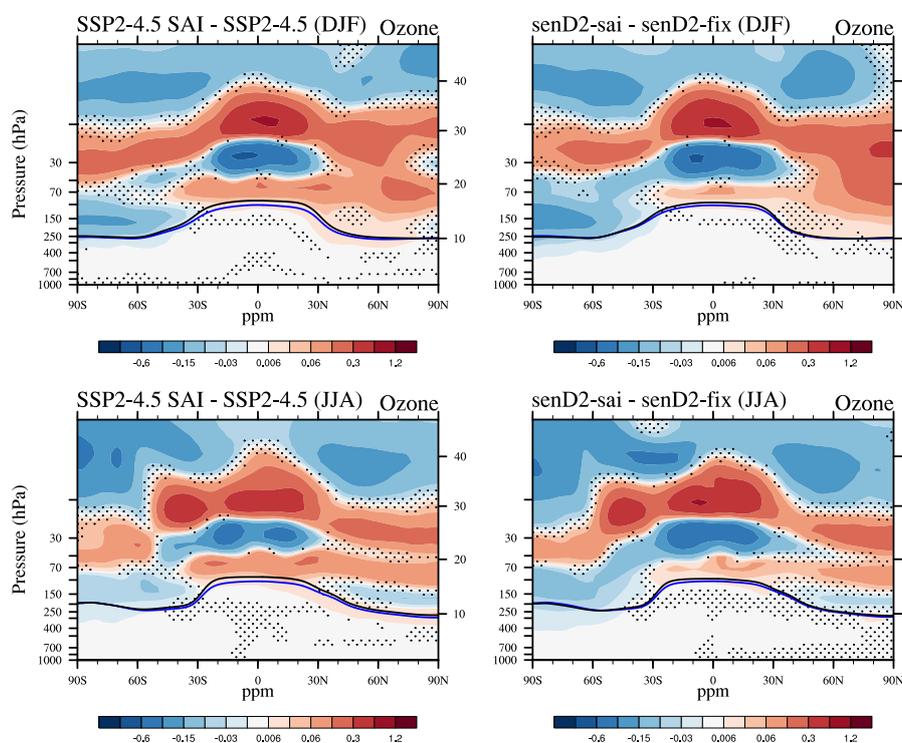
Figure A3. Differences of zonally averaged ozone mixing ratios (ppm) for December/January/February (top row) and June/July/August (bottom row), between SSP2-4.5 SAI and SSP2-4.5 (left) and senD2 and senD2-fix in 2070 – 2080. The lapse rate tropopause is indicated as a black line for the control experiment and a blue line for the SAI cases (left and middle panels). Areas of non-significant difference at the 95th % level to the control are marked as small black dots.